

Dagmawi Wendwessen Gebrehiwot

**Assessment of Critical Energy Release
Rate of Plywood under Mode-II
Delamination**



FRP++

Advanced structural analysis and
design using composite materials

Master Dissertation
European Master Advanced Structural Analysis
and Design using Composite Materials

Work developed under the supervision of
Professor Bruno CASTANIE
Doctor Hajer HADIJI and Doctor Joel SERRA



Funded by
the European Union

DECLARATION

Name: Dagmawi Wendwessen Gebrehiwot

Email: www.dagiwonde91@gmail.com **Phone number:** +33751111434

Citizen Card Number: XXXXXXXXXXXXXXXXXXXXXXX

Title of the Thesis: Assessment of Critical Energy Release Rate of Plywood under Mode-II Delamination

Supervisors:

Professor Bruno CASTANIE

Doctor Hajer HADIJI and Doctor Joel SERRA

Year of Conclusion: 2023

Master Course in Advanced Structural Analysis and Design using Composite Materials

THE ENTIRE REPRODUCTION OF THIS THESIS IS AUTHORIZED ONLY FOR RESEARCH PURPOSES, UPON WRITTEN DECLARATION BY THE INTERESTED PERSON, WHICH IS COMMITTED TO.

University of Toulouse III Paul Sabatier, 04/09/2023

Signature:

ACKNOWLEDGEMENTS

I would like to express my sincere gratitude and praise for the most high and respected Almighty GOD, son of David, son of our lady saint virgin MARY, our lord and saviour JESUS CHRIST of Nazareth for making my life filled with his mercy and love and helping me through all the impossible seeming problems.

I am sincerely grateful to my priceless family, my dad Wendwessen Gebrehiwot, my mom Elisabeth Alayu, my sisters Nitsuh and Mahder, it is truly a blessing to have a family like you that can give an immense support and energy with all the prayers and optimism regardless of distance. I dedicate this work to this invaluable family of mine. Without their encouragement and motivation, I would not have been able to complete this journey.

I would also like to thank my teachers at New era School, CMMTS, University of Gondar, and friends. Special thanks goes to Wendwessen Tibebu, Yohannes Ezezew with his wife Rekek Alemayehu, Kibrom H., Mrs. Tsega Yesgat(mommiye), Michael Samson, Samuel Alayu Assafa(Including all the family members; ABAYE ENWEDHALEN) , Mrs. Askale, Moges Bekele, Aman Menkir, Betsha Senay, Endalk Simegn, Eyob Teshome, Natnael Nigussie, Bereket Bogale, Merhawi Junior, Mrs. Almaz Gebrehiwot(beloved aunty with all the family members; SIYUME ENWEDHALEN), Dagim Abdisa, Tenagnework Taye(Mediye), Asayu Kebede(we will always miss you Asiye), Hana Kebede(hanicho), Etsub Gebremeskel, Dagne Negewo and his wife Tiwobesta Getachew, Nebiyu Merekelgn, Samuel Befekadu, Habtamu Tilahun, Million Angesom, Fikadu Reta Alemayehu(YessEthiopia), Abel Belachew, Liyou Zewdie, Caballe and Vila family, Doctor Aniol Bosch, Shewit Atnafu, Tamrat Zeleke, Toulouse Ethiopian community and many others for their valued support to this master and my future career.

I am deeply grateful to my supervisor Doctor Hajer HADIJI and Doctor Joel SERRA for their unwavering support and guidance throughout my master's dissertation. Their expertise and patience have been invaluable to me and have played a crucial role in the success of this thesis. I highly appreciate the ICA laboratory technicians, Professors, PhD students, Post-doctoral and other staff members for their impacting support to facilitate my dissertation inside the laboratory.

I would like to extend a special thanks to the head of our FRP++ master's dissertation inside Institute Clement Ader (ICA), Professor Bruno CASTANIE, for his fatherly support and unexplainable help for those ditches of professional and financial problems I was facing.

Technically, God Almighty assigned this invaluable professor letting him to think with his conscience, to give all he got getting me out of those dark and hard days which were straits against my path. Thank you so much for all you did. Without you, this work would not have been possible. I would not be able to thank you enough, and I pray God Almighty to rewards you abundantly. I appreciate Prof. Jose Sena Cruz, Prof. Cristina Barris and Mrs. Maria Goretti helping me to apply for Banco Santander's Masters-tuition grants as I won ranked the second from the participants. All the FRP++ first edition colleagues, it was great meeting and learning with you. Last but not least, I appreciate the entire distinguished professors in AMADE and the entire MSc-FRP scholarship board for accepting me to be part of this monumental academic path. "...But with God all things are possible." Mark 10:27 እግዚአብሔር ይችላል!!!

ÉVALUATION DU TAUX DE LIBÉRATION D'ÉNERGIE CRITIQUE DU CONTREPLAQUÉ SOUS DÉLAMINAGE DE MODE II

RESUME

La caractérisation du comportement à la rupture des matériaux est un facteur important à prendre en compte dans la conception des structures afin de mieux comprendre les différents scénarios de rupture au cours de leurs utilisations. Bien que les matériaux naturels soient disponibles et durables, avec un processus de fabrication simple pas cher, leur comportement est relativement complexe par rapport aux matériaux synthétiques en raison de la non-homogénéité de leur microstructure et de leur comportement mécanique. Pour cette raison, peu d'études de mode II ont été réalisées jusqu'à présent sur des matériaux naturels tels que le bois contreplaqué. Ce travail porte sur la caractérisation de la rupture du contreplaqué en déterminant le taux de restitution d'énergie critique sous un mode II de chargement, à l'aide de l'essai de flexion à quatre points. Deux catégories d'échantillons avec des orientations de fibres de $0^\circ/0^\circ$ et $0^\circ/90^\circ$ ont été étudiées. L'originalité dans ce projet est l'application de la technique DIC (Digital Image Correlation) pour éviter le contrôle manuel de la longueur de fissure lors de la réalisation de l'essai, ce qui permet de gagner du temps tout en obtenant des données de qualité par rapport aux méthodes conventionnelles. Les éprouvettes ont été préparées avec un mouchetis sur leur section d'épaisseur, face aux caméras. Les caméras détectent donc le mouvement des taches du mouchetis. Le logiciel VIC-3D permet par ensuite de calculer le déplacement de l'éprouvette et la longueur de la fissure. Deux méthodes de calcul, basées sur la complaisance de l'éprouvette et la théorie des poutres ont été appliquées : La méthode de Calibration de Complaisance (CCM) et la méthode Complaisance Basée sur la théorie des poutres (CBBM). Un script Python a été utilisé pour générer les courbes de résistance ($G_{IIc} = f(a)$), à partir des courbes charge-déplacement. Pour valider les résultats, une comparaison a été effectuée entre les résultats du CCM et du CBBM, et une bonne cohérence a été constatée. Ceci confirme que la technique DIC combinée à l'essai de flexion en quatre points décrit bien le comportement de rupture en mode II du matériau contreplaqué étudié. En outre, l'étude des surfaces de rupture a été réalisée pour mieux expliquer les résultats des deux types d'éprouvettes.

MOTS-CLES: Courbe-R; Bois Contre-plaqué; Complaisance; Analyse expérimentale.

ASSESSMENT OF CRITICAL ENERGY RELEASING RATE OF PLYWOOD UNDER MODE-II DELAMINATION

ABSTRACT

Characterization of the failure behaviour of materials is an important factor to consider in the design of structures to better understand various failure scenarios during application. Despite natural materials are abundant and sustainable, let alone their simple and cheap production process, their investigation becomes relatively complex compared to synthetic ones due to their non-homogenous microstructure and mechanical behaviour. Therefore, few studies have been made so far on natural materials like plywood. This work addresses plywood fracture characterization through determining critical energy release rate under mode II loading using the Four-Point End-Notched Flexure test. Two categories of specimens with ply fibre orientations of $0^\circ/0^\circ$ and $0^\circ/90^\circ$ have been studied. Unlike previous works, this project adopts DIC (Digital Image Correlation) technique to avoid manual monitoring of crack length while conducting the test which makes the campaign time efficient while having quality data compared to those conventional methods. The specimens were prepared with speckles on its thickness side that is faced to the stereo cameras. Cameras will therefore detect the motion of speckles. Hence, using VIC-3D software, the displacement of the specimen and the crack length can be calculated. Two appropriate data reduction methods based on specimen compliance and beam theory were implemented: Compliance Calibration Method (CCM) and Compliance-Based Beam Method (CBBM). Both methods do not need to conduct extra experiments to assess the elastic characteristics. Python script was used to generate the relevant Resistance-curves ($G_{IIc} = f(a)$) from experimental load-displacement curves. To validate the results, a comparison was made between the CCM and CBBM results, and a good agreement was found. This confirms that the DIC technique combined with Four-Point End-Notched Flexure test describe well the mode II failure behaviour of the studied plywood material. Furthermore, investigation of fracture surfaces was done to better explain the results of the two categories of specimens.

KEYWORDS: Fracture toughness; Plywood; Compliance; Experimental analysis.

TABLE OF CONTENTS

1. CONTENTS

Acknowledgements	III
Résumé.....	V
Abstract	VI
Table of Contents	VII
List of Figures	IX
List of Tables.....	XII
List of Abbreviations and Symbols.....	XIII
1. Introduction.....	1
1.1. The EMJM FRP++	1
1.2. Institute Clement Ader (ICA).....	2
1.3. Objective of the Dissertation/internship project.....	3
2. Literature review	5
2.1 Introduction	5
2.2 Introduction to the application of wood in the aeronautic and automotive applications 5	
2.3 Characteristics of wood materials.....	7
2.3.1 Wood and wood composites	7
2.3.2 Structure and composition of wood	9
2.4 Failure modes	11
2.5 Mode-II fracture toughness	12
2.5.1 Experimental tests of the mode-II delamination	12
2.5.2 Calculation of the strain energy release rate and R-curve according to different test set-ups.....	14
2.5.2.1. Compliance Calibration Method.....	15
2.5.2.2. Beam theory analysis	15
2.5.2.3. Compliance based beam method (CBBM)	16
2.5.3 Previous works on the investigation of mode-II fracture toughness of wood....	17
2.6 Conclusion	21

3.	Materials and Methods.....	23
3.1	Introduction	23
3.2	Specimen design and manufacturing.....	23
3.2.1	Dimensions of specimens.....	24
3.2.2	Manufacturing process of plywood plates	25
3.2.3	Formation of pre-crack.....	29
3.2.4	Cutting out the specimens	29
3.2.5	Preparation of the specimens for the 4ENF test.....	31
3.3	Four-point end notch flexure test set-up.....	33
3.3.1	Test equipment	33
3.3.2	Test set up and procedures	37
3.4	Post-processing of experimental data	38
3.4.1	VIC-3D calculations.....	38
3.4.2	Curves of the force-displacement.....	41
3.4.3	Crack propagation calculation.....	42
3.4.4	Calculation of the strain energy releasing rate	45
3.4.5	Infrared thermography.....	48
3.5	Conclusion	48
4.	Results and Discussion	49
4.1	Introduction	49
4.2	Load-displacement responses	49
4.3	Resistance-curves	50
4.4	Discussion.....	52
4.4.1	Comparison of the fracture toughness calculated with CCM and CBBM.....	53
4.4.2	Comparison of mode II delamination between 0°/0° and 0°/90° interfaces	53
4.4.3	Mode II and mode I fracture toughness	56
4.5	Conclusion	57
	References	59

LIST OF FIGURES

Figure 1.1: MSc-FRP 1 st edition.....	2
Figure 1.2: Institute Clement Ader.....	3
Figure 2-1: Pioneering aviation projects: (a) The twin-propeller-driven Avion III [7], and (b) Model of Wright Flyer [8].....	6
Figure 2-2: De Havilland DH.98 Mosquito [1].....	6
Figure 2-3: “Costin Nathan Le Mans” racing car [4].....	7
Figure 2-4: (A) Douglas fir, (B) sugar pine, (C) redwood, (D) white oak, (E) American sycamore, and (F) black cherry wood. Each image shows (from left to right) transverse, radial, and tangential surfaces) [9].	7
Figure 2-5: Types of plywood [9].	9
Figure 2-6: Transverse section of tree trunk [9].....	10
Figure 2-7: Types of cells present in hardwoods and softwoods [9].	10
Figure 2-8: Basic Delamination modes [10].	11
Figure 2-9: Mixed mode fracture [10].....	12
Figure 2-10: Four test methods for measuring interlaminar fracture toughness [16].	13
Figure 2-11: Free body diagram of the 4ENF specimen test [20].....	17
Figure 2-12: Calculation of the fracture toughness of solid wood by the three methods proposed by Yoshihara [22].....	18
Figure 2-13: R-curves obtained by De Moura et al. for Pinus pinaster wood specimens [20].	19
Figure 2-14: Geometric ELS test fixture adopted by El Moutaphaoui et al. [27].....	20
Figure 2-15: R-curves obtained by El Moutaphaoui et al. [27] using ELS test for plywood specimens.	20
Figure 3-1: 0°/0° Specimen.....	23
Figure 3-2: 0°/90° Specimen.....	24
Figure 3-3: 4ENF specimen dimensions	25
Figure 3-4: Overall manufacturing process of plywood [28].....	25
Figure 3-5: Peeling operation [28].	26
Figure 3-6: Veneer numbering (ENSAM Cluny, France).....	27
Figure 3-7: Glue Application on the veneers	27
Figure 3-8: Plies inside the press machine ready to be pressed.	28
Figure 3-9: Press machine	28
Figure 3-10: Arrangement of 0°/0° specimens in veneers plate.	30

Figure 3-11: Arrangement of 0/90/0 specimens in veneers plate.....	31
Figure 3-12: Spraying of specimens.....	32
Figure 3-13: Speckles on the specimen and faces of rollers.	32
Figure 3-14: 5900 series universal testing systems-Instron.	33
Figure 3-15: Experimental setup of a four-point bending test	34
Figure 3-16: Test set-up assembly with the specimen	34
Figure 3-17: (a) Area of interest (AOI) and subset in a reference image; (b) schematic presentation of a reference subset before deformation and the corresponding target subset after deformation [30]......	35
Figure 3-18: Calibration process	36
Figure 3-19: Infrared thermography device and Dual camera setup with a blackout panel as a background of the specimen.....	36
Figure 3-20: Launching of the pre-liminary test.	38
Figure 3-21: Stereo system calibration.....	39
Figure 3-22: Region for the analysis and start point.	39
Figure 3-23: Meshing the region with respect to subset and step parameters.....	40
Figure 3-24:Threshold settings.....	40
Figure 3-25: VIC-3D Analysis in progress	41
Figure 3-26:Displacement points on the specimen	42
Figure 3-27: Displacement extraction plot.....	42
Figure 3-28: Crack propagation with noise.....	43
Figure 3-29: Sigma value adjustment for a clear crack tip	43
Figure 3-30: Example of videos extracted from VIC-3D software.....	44
Figure 3-31: Python code used for crack monitoring.....	44
Figure 3-32: Text file generated by the python script giving the crack length in pixels	45
Figure 3-33: Example of the evolution of the specimen compliance as a function of the crack length.	46
Figure 3-34: Example of the R-curve obtained with the Compliance Calibration Method.	47
Figure 4-1: Evolution of the force with the displacement for (a) 0°/0° and (b) 0°/90° specimens.	50
Figure 4-2: R-curves for (a) 0°/0° and (b) 0°/90° specimens obtained with Compliance Calibration Method.	51
Figure 4-3: Mean values of GIIC obtained with CCM and CBBM for (a) 0°/0° and (b) 0°/90° specimens.	53

Figure 4-4: Side view of the delamination growth in $0^{\circ}/0^{\circ}$ interface.	55
Figure 4-5: Side view of the delamination growth in $0^{\circ}/0^{\circ}$ and in (b) $0^{\circ}/90^{\circ}$ interface.	55
Figure 4-6: Delamination path for (a) $0^{\circ}/0^{\circ}$ and (b) $0^{\circ}/90^{\circ}$ specimens [36], [37].	55
Figure 4-7: Fracture surfaces of a specimen with a $0^{\circ}/0^{\circ}$ interface.	56
Figure 4-8: Fracture surfaces of a specimen with a $0^{\circ}/90^{\circ}$ interface.	56

LIST OF TABLES

Table 2-1: Stability of mode II tests [17].	13
Table 2-2: Advantages and disadvantages of the four specimen configurations.	14
Table 4-1: Mean critical strain energy release rates of 0°/0° specimens.	52
Table 4-2: Mean critical strain energy release rates of 0°/90° specimens.	52
Table 4-3: Mode I and mode II fracture toughness of poplar plywood compared to wood and composite materials from the literature.....	57

LIST OF ABBREVIATIONS AND SYMBOLS

Abbreviations

ENF	End Notched Flexure test
ELS	End Load Split test
4ENF	Four-point End Notched Flexure test
DIC	Digital Image Correlation
CCM	Compliance Calibration Method
CBBM	Compliance Based Beam Method

Symbols

l	specimen length
b	specimen width
h	specimen thickness
L	half distance between the two outer rollers
P	load applied on the specimen
δ	vertical displacement of the specimen
a	crack length
a_0	initial crack length
C	compliance
C_0	initial compliance
G_{IIc}	critical strain energy release rate in mode II
G_{Ic}	critical strain energy release rate in mode I
E	Young's modulus along the longitudinal direction
I	moment of inertia of a 4ENF specimen
X	specimen length direction
Z	specimen thickness direction

THIS PAGE WAS INTENTIONALLY LEFT BLANK

1. INTRODUCTION

1.1. The EMJM FRP++

The FRP++ is a European master program in advanced structural analysis and design using composite materials. With a focus on mechanics and modelling, analysis and design, mechanics and diagnosis, inspection, diagnosis, repair and strengthening, sustainability and life cycle analysis, and other key issues facing the composites industry, the FRP++ offers an advanced integrated educational program. In order to provide a top-notch educational proposal focused on a multidisciplinary understanding of structural Composites through the involvement of experts from complementary fields (engineers, materials scientists, and others). The master brings together the diverse expertise of top European higher education institutions in the related fields. On my side, this master's Programme has two parts: Coursework held from October 1, 2022, until March 2023 at the University of Girona; and the Dissertation has been going from March 2023 until September 30, 2023, at the Institut National des Sciences Appliquées de Toulouse/University Toulouse III Paul Sabatier. My dissertation involves an internship with Institute Clement Ader (ICA), TOULOUSE, which works closely with the institutions mentioned above.

The FRP++ lasts for one academic year (60 ETCS), after which a double master's degree is granted. It is distributed among partners on a rotational basis. Students do their dissertation at a different place from where they complete their courses. English is the medium of teaching and testing.

Students who receive a top-notch education will be prepared to compete in a highly competitive market, such as construction, aerospace and aeronautics, automotive, and wind energy, among others, where Composites are fundamental. This will be accomplished by gaining cutting-edge knowledge on structural Composites in a research-driven environment, maintaining close collaboration with industry, and placing a significant emphasis on solving practical problems. The FRP++ integrates the most recent developments in research with the growth of activities pertaining to professional practice.



Figure 1.2: MSc-FRP 1st edition

1.2. Institute Clement Ader (ICA)

Toulouse, France is a home to the well-known research laboratory Clément Ader Institute (ICA) named after the pioneering aeronautical engineer Clement Ader. It is a component of the CNRS UMR 5312 and concentrates on the study of mechanical processes, systems, and structures, with an emphasis on the energy, transportation, aerospace, and space sectors. The ICA carries out considerable research in several fields, such as behaviour modelling, instrumentation, and structural durability. They put a lot of attention on composite material research since it's important for modern engineering applications. The institution has a long history of publications and has received media attention for its work in the fields of materials science and mechanical engineering. The Clément Ader Institute's primary core is based in Toulouse's ESPACE CLEMENT ADER, which is part of the Montaudran Aerospace complex. In order to further increase its presence and research operations, the institution now maintains offices in Tarbes and Albi.

To complete multidisciplinary research initiatives, ICA works in conjunction with a variety of academic and business partners. Within the institution, the Department of Materials and Composite Structures (MCS) at ICA works on areas such as composite materials, damage characterization, numerical modelling, optimization, machining, nonlinear behaviour, vibration dynamics, and assembly processes. The MCS team collaborates closely with companies like Thales Alenia Space, Airbus, CEA, CNES, ESA, ONERA, and SAFRAN on initiatives that enhance the aerospace and associated sectors.



Figure 1.2: Institute Clement Ader.

1.3. Objective of the Dissertation/internship project

The objective of the thesis is to focus on the experimental determination of the delamination behaviour of plywood under mode II loading. The aim is to have enough understanding and data to be able to model the behaviour of plywood structural components that could be used in aerospace or automotive industry.

The material of this study is poplar plywood. The project proposes to determine the interlaminar fracture toughness of poplar plywood. Two different interfacial fibre orientations are to be characterized. To this end, two configurations of poplar plywood specimens will be studied: $0^{\circ}/0^{\circ}$ and $0^{\circ}/90^{\circ}$. The study will include a bibliographic part, the manufacturing of the test specimens, the tests as well as the results interpretation.

The overall road map of this project starts by reviewing several literatures which are related to our objective and then analysing different suitable configurations of experiments with their possible outcomes and drawbacks. Further study on the 4-ENF test would be considered. Then, the specimens to test would be manufactured. Next, the chosen mode II fracture test will be realized on the manufactured specimens. Finally, a data reduction procedure must be done in order to obtain the mode II fracture toughness results, which will be explained by investigation of the tested specimens fractured surfaces.

THIS PAGE WAS INTENTIONALLY LEFT BLANK

2. LITERATURE REVIEW

2.1 Introduction

Understanding the mechanics of certain materials and structures depends heavily on mode-II fracture studies. When there is a relative sliding or shearing motion between two surfaces of a material, perpendicular to the direction of the applied force, a fracture known as a mode-II fracture takes place. Another name for it is in-plane shear fracture. Giving a scientific justification for a material assures how that material is fit for the intended application area. This mitigates the worst-case scenarios on structures during their service life increasing integrity of members.

The study of Mode-II fracture offers important insights into how materials behave when subjected to shear stress. For natural materials like wood, quality monitoring is crucial in order to guarantee the durability and integrity of that utilized type of wood. As properties of wood varies from specimen to specimen, conducting a test and getting an approximate behaviour would be recommended.

2.2 Introduction to the application of wood in the aeronautic and automotive applications

Throughout the past, wood and its composites have proven their mechanical performance in many aeronautic and automotive applications [1]–[6].

Wood was a key component in aircraft construction in the early days of aviation, including the pioneering engineer Clement Ader's heavier-than-air motorized aircraft, which was built of wood and fabrics, and had the first flight in 1890 (Figure. 2.1a) [7]. In 1903, the Wright brothers, have manufactured the world's first sustained and controlled heavier-than-air powered flight using wood and fabric tied together with twine [8] (Figure 2.1b). By 1912, manufacturers were constructing aircraft with laminated wooden fuselages using monocoque construction. Albatross fighters from World War I and Amelia Earhart's famous Lockheed 5B Vega are two examples of planes that had this design [8].

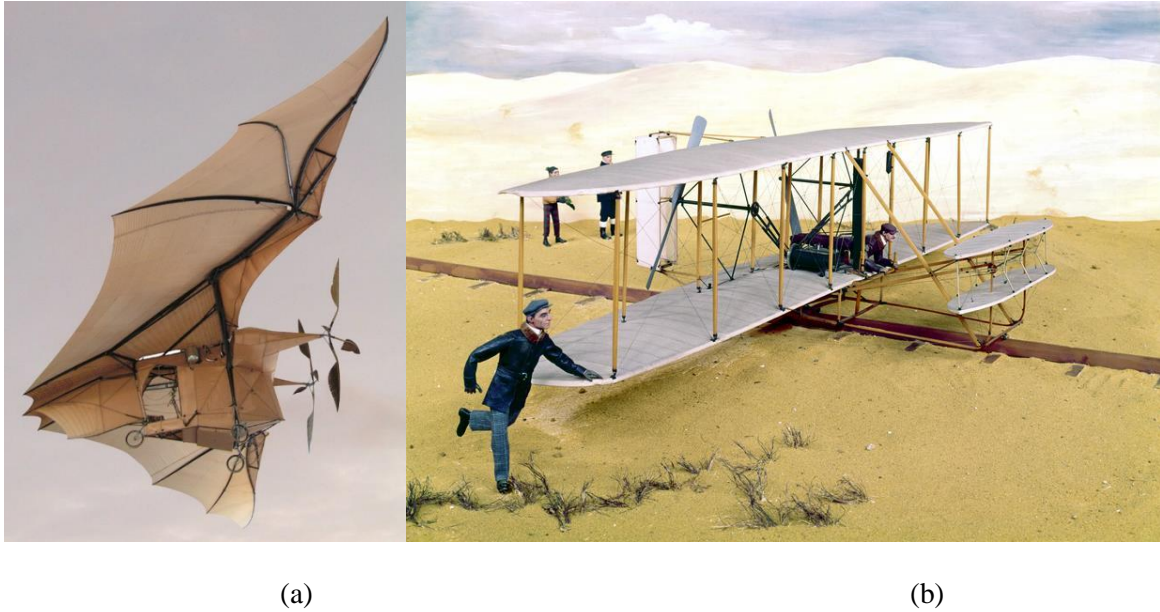


Figure 2-1: Pioneering aviation projects: (a) The twin-propeller-driven Avion III [7], and (b) Model of Wright Flyer [8].

The de Havilland Mosquito, is a prime example of how important wooden aircraft were during World War II [1]. The de Havilland Mosquito, commonly referred to as the "Wooden Wonder," was a flexible and popular aircraft made largely of wood products such as plywood, balsa, birch, and spruce. It had several functions and was used in several operational areas, including Europe, the Mediterranean, the Atlantic, and the Far East. Some aviation specialists even rank the Mosquito above the venerable Supermarine Spitfire and the Hawker Hurricane as the best British aircraft of the conflict. The Mosquito's wooden structure has several benefits. Compared to metal airplanes, which were frequently in poor supply during the war, it allowed for speedier manufacture and simpler construction.



Figure 2-2: De Havilland DH.98 Mosquito [1].

In the automotive industry, Wood was also a material often used to make some car's components.

We can cite the example of the "Costin Nathan" racing car (Figure 2.3), which competed in the Le Mans 24-hour race in France in 1967 [4]. Its designer, the English engineer Franck Costin, chose plywood for the chassis of his car to make it lighter, weighing only 450 kg.

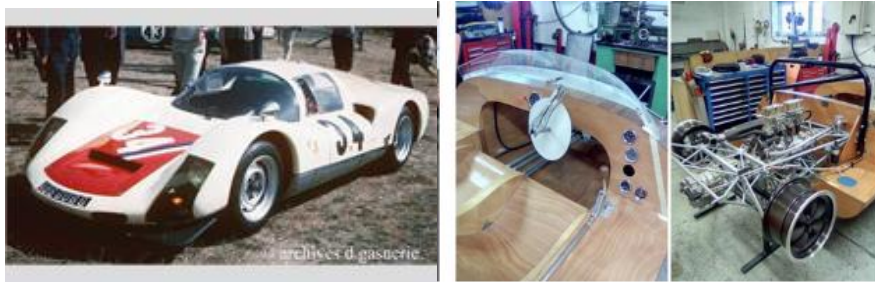


Figure 2-3: "Costin Nathan Le Mans" racing car [4].

2.3 Characteristics of wood materials

2.3.1 Wood and wood composites

Wood is a plentiful natural resource presented in trees and other plants. Humans have been using wood since the beginning of time, and despite competition from other materials, it still plays a crucial role. It serves as a raw material for panels, paper, chemicals, plywood, timber, and other products. Gymnosperms (softwoods) and angiosperms (hardwoods) are the two principal plant species of wood. Figure 2.4 shows some examples of solid wood.

Moreover, wood can be combined with other materials like the glue to form wood composites such as LVL and plywood.

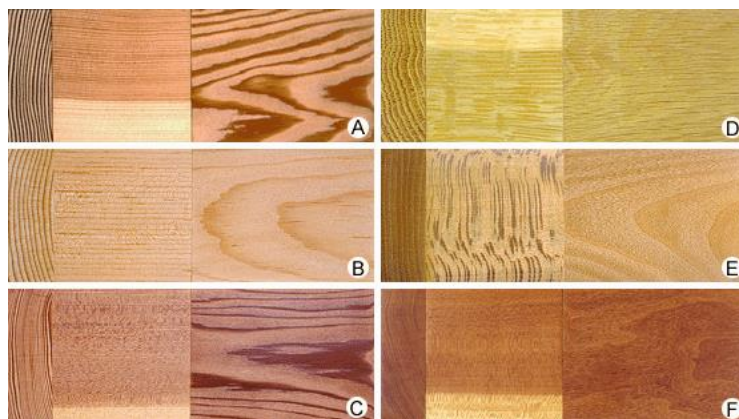


Figure 2-4: (A) Douglas fir, (B) sugar pine, (C) redwood, (D) white oak, (E) American sycamore, and (F) black cherry wood. Each image shows (from left to right) transverse, radial, and tangential surfaces) [9].

In fact, Laminated Veneer Lumber (LVL) and plywood are made from glued wood veneers. The main distinction is that LVL has parallel grain, while plywood is composed of cross-ply

veneers perpendicular to one another. In plywood materials, one or more veneers are glued to the back and front of a central veneer layer, or a core made of timber strips to create plywood, a panel product. Most of the plywood is made entirely of veneers; lumber-core plywood is very rare to be made (Figure 2.5). After the adhesive has been applied between the veneers, the panel is put together and pressed. For plywood intended for internal use, urea-formaldehyde is used as an adhesive, and phenol-formaldehyde for plywood intended for outdoor use. Phenol-formaldehyde glue may create joints that are more resistant to weather, microbes, cold water, hot water, boiling water, saltwater ("marine" plywood), steam, and dry heat than the actual natural wood itself. For all-veneer plywood, the thickness varies from 3 mm (or 0.12 inches) to 30 mm (1.2 inches) for lumber-core plywood [9].

Plywood can be also produced in curved shape (moulded plywood), which is used for boats, furniture, and other things in addition to flat panels. Veneer sheets are bent and adhered together to create moulded plywood; by using either fluid pressure applied using a flexible "bag" or "blanket" of impermeable material or curved forms in a press.

Compared to solid wood, laminated wood can offer some benefits such as its adaptability to complex shapes, its dimensional stability. In fact, panels with complex or curvature geometry can be difficult to create from solid wood. Also, a selection of the veneers used in manufacturing plywood panels can be done to eliminate veneers with knots or flaw, to ensure an optimal quality of the final plywood panel.

The adaptability of wood and its many desirable features, including high strength for its weight, workability, and aesthetic appeal, enable such broad use. However, there are some unfavourable qualities in wood as well. For example, it may burn and decompose. It absorbs moisture and changes size depending on how much moisture it has. It is hygroscopic. Wood is also a variable-quality biological product. It is crucial to comprehend the complicated nature of this material in order to lessen the consequences of these inherent unfavourable features, as well as to make effective use of the many existing wood products and wood-producing plant species.

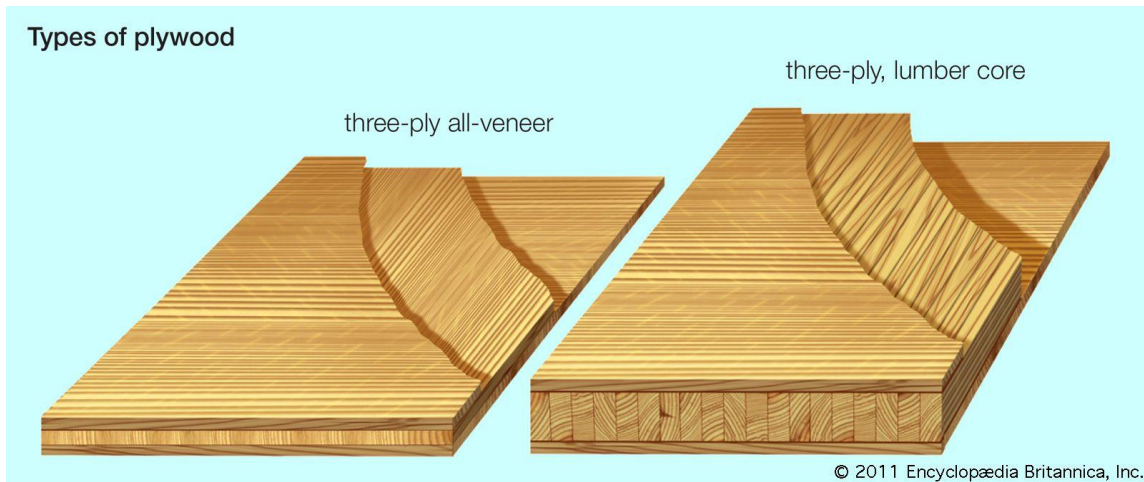


Figure 2-5: Types of plywood [9].

2.3.2 Structure and composition of wood

Three components: pith, wood, and bark constitute the transverse section (cross section) of a tree trunk, as depicted in Figure 2.6. Wood may be identified in the tree trunk by the presence of yearly or growth ring-style concentric layers. During each season of development in temperate climates, one growth ring is typically created, while false rings may also exist and in certain situations, some rings may be locally discontinuous. The number of growth rings, as counted in a transverse section close to the ground, may be used to determine the age of a tree. At a microscopic scale, the wood is made up of cells such as: Tracheid, vessel members, fibers, and parenchyma. Tracheid and parenchyma are presented in softwoods, whereas vessel members, fibers, and parenchyma are the principal cells of hardwoods (Figure 2.7).

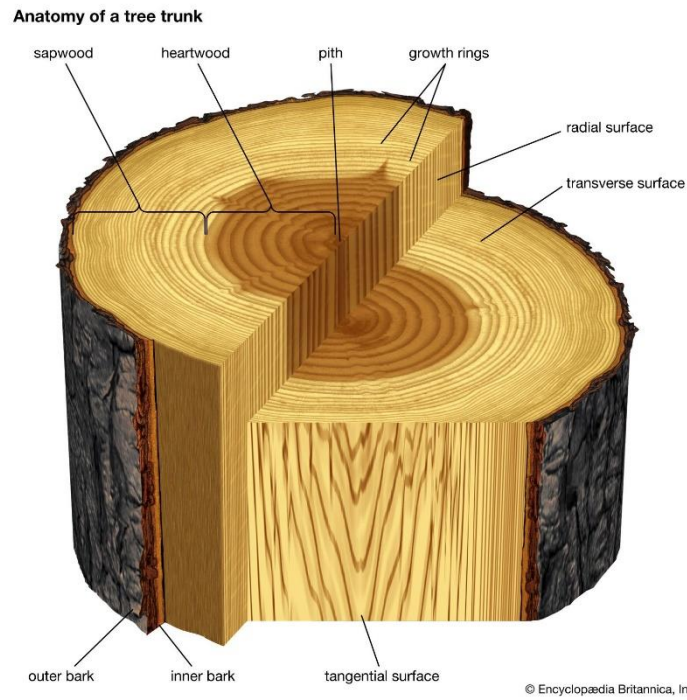


Figure 2-6: Transverse section of tree trunk [9].

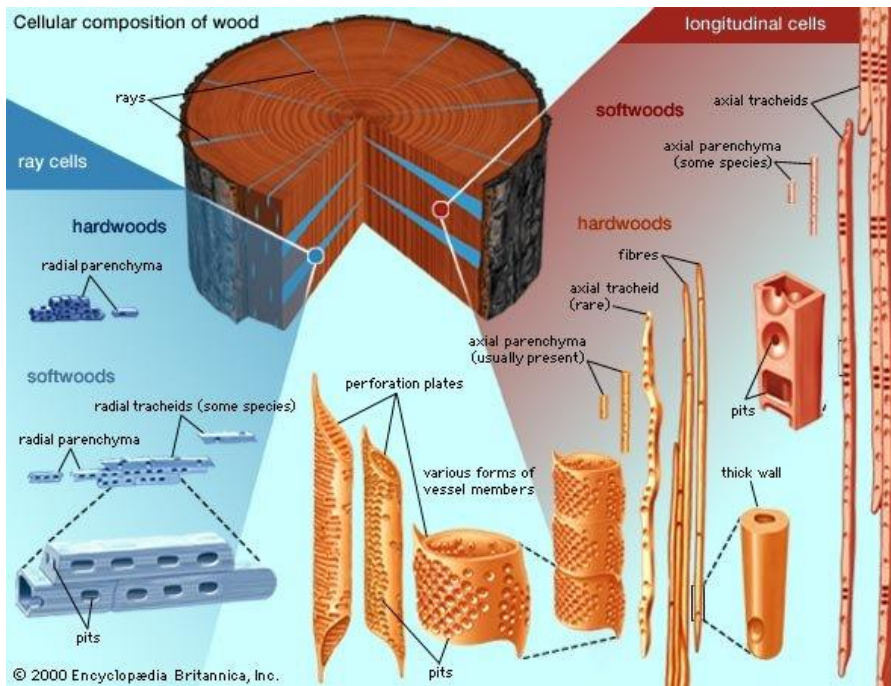


Figure 2-7: Types of cells present in hardwoods and softwoods [9].

2.4 Failure modes

Three modes of failure behaviour can be distinguished: mode I, mode II and mode III (Figure 2.8).

Mode I refers to the separation of layers along the plane parallel to the surface interface. It occurs when there is a tensile force perpendicular to the specimen direction, causing the layers to separate from each other. Mode II delamination involves the delamination of layers along the plane parallel to the surface but with a shear force applied parallel to specimen direction. This type of delamination occurs when there is a sliding motion between the layers. Factors such as improper adhesive bonding, excessive or insufficient glue, or fasteners placed too close to the edges can contribute to mode II delamination. Mode III delamination refers to the separation of layers along the plane perpendicular to the specimen surface. Mode III delamination is less common compared to modes I and II [10].

When many different modes of crack propagation occur in a material at the same time, this is referred to as mixed mode fracture. This mixed mode can be encountered when a specimen is exposed to complicated loading conditions.

We note that his project will focus only on the characterization of the studied plywood under mode-II delamination. Indeed, the fracture behaviour of plywood, particularly delamination, is a critical concern in industries like aerospace and automotive, because delamination can lead to stiffness reduction and premature failures.

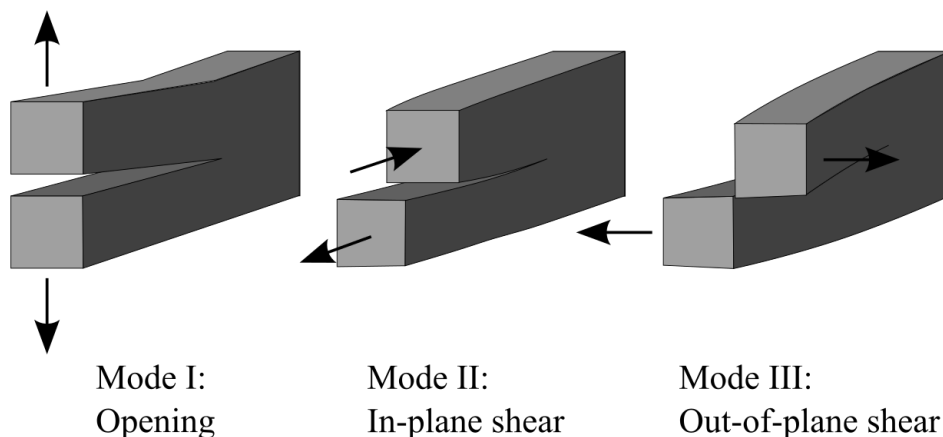


Figure 2-8: Basic Delamination modes [10].

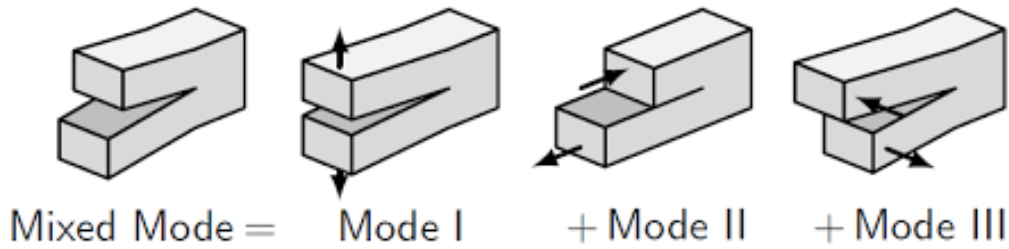


Figure 2-9: Mixed mode fracture [10].

2.5 Mode-II fracture toughness

As mentioned above, we are interested in the characterization of mode II delamination behaviour of plywood materials. For this reason, the main experimental and data reduction methods to calculate the mode II fracture toughness are summarized in this section.

2.5.1 Experimental tests of the mode-II delamination

Numerous efforts have been made to establish standard test methods for the evaluation of the interlaminar fracture toughness of carbon fibre reinforced composites by researchers and composite societies, such as the European Structural Integrity Society (ESIS), the American Society for Testing and Materials (ASTM) group, and the Japanese Industrial Standards group (JIS) [11]. From the different mode II test methods, we can cite the three most used test configurations: ENF, ELS, and 4ENF tests (Figure 2.10).

The ENF (End Notched Flexure test), standardized as ASTM international standard D7905/D7905M-14 for composite materials, is the most widely used [12]. In ENF test, the specimen, pre-cracked at the interface to characterise, is on a 3-point bend fixture. The test is easy to perform, but the crack propagation is only stable when the condition ($a_0/L > 0.7$) is satisfied. This condition is reduced for ELS test (End Load Split test), standardized as ISO 15 114 [13]. In this test, the specimen is blocked on one side and loaded on the other side, and the condition ($a_0/L > 0.55$) must be satisfied to obtain stable crack propagation. Although the stability condition is reduced compared to ENF test, ELS test is much more complicated in its set up. In 1999, Martin and Davidson [14] proposed the 4ENF test (Four-point End Notched Flexure test). In this test, the pre-cracked specimen is positioned on two support points and the load is applied by two loading points. This test is not standardized, but its advantage is that it always ensures a stable crack propagation without any conditions on the specimen dimensions or shape.

Tanaka et al. [15] also suggested the over notched flexure (ONF) test in addition to the three tests already listed (Figure 2.10). The test fixture for the ONF test is the same as that for the ENF test, and it likewise produces steady fracture propagation. On the other hand, the loading point in both the 4ENF and ONF tests is above the crack.

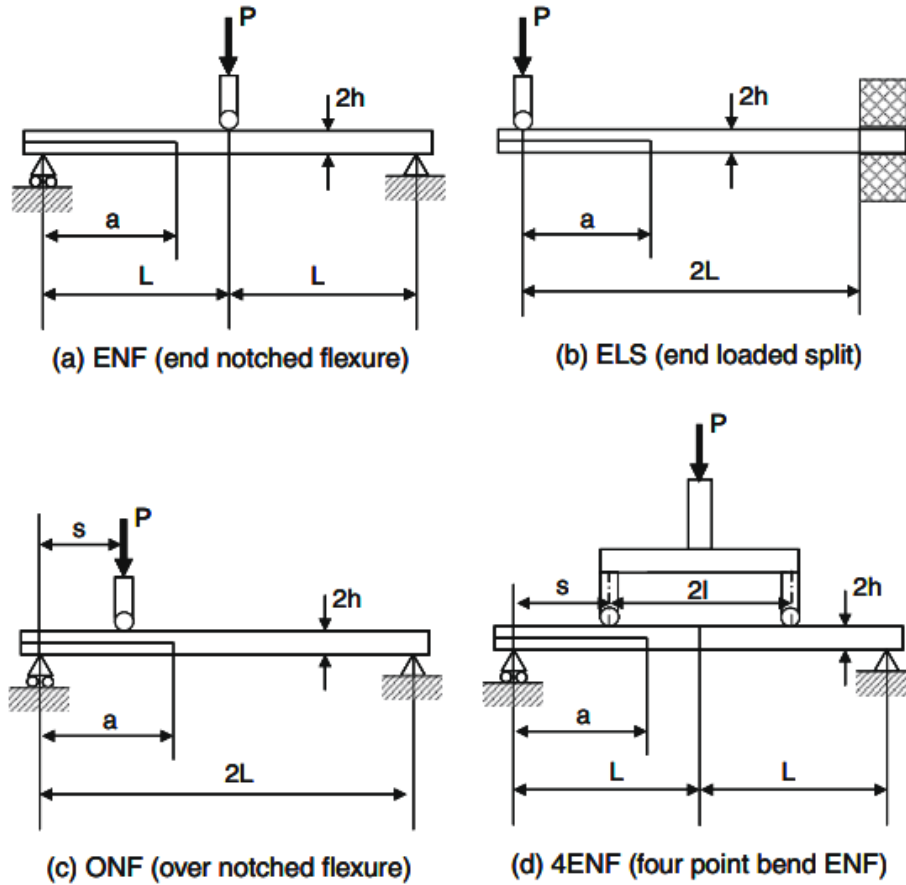


Figure 2-10: Four test methods for measuring interlaminar fracture toughness [16].

Stability of crack propagation is a major factor to choose between test configurations. Below, table 2.1 shows the expected stability from the above detailed test methods.

Table 2-1: Stability of mode II tests [17].

Specimen	Expected stability
ENF	Unstable $a/L > 0.7$
ELS	Stable $a/L > 0.55$
ONF	Stable
4ENF	Stable

There are two advantages of a stable fracture propagation during a mode II loading test. First, it allows for the determination of the material's R-curve, which may be useful for enhancing

damage tolerance. Second, and perhaps more crucial for the standardization process, a steady R-curve makes it possible to determine the reliability of the initiation values [17].

To conclude, the mode II characterization tests have advantages and difficulties particularly in dealing with unstable crack propagation for this reason, the researchers try to select the test that respect most of the objectives below:

- Pure mode-II loading
- Stable crack propagation
- Best suited way of crack monitoring without interrupting and delaying the test
- Less complexity of test configuration
- Consistency of results
- Efficient data reduction method
- Lesser time to run the test
- Validation of results

For our work, we chose the 4-ENF test, since it is the test configuration that ensures stable crack propagation without limitations on the specimen dimensions. This test is adopted for the present study. Below, a table shows the advantages and disadvantages of the test methods.

Table 2-2: Advantages and disadvantages of the four specimen configurations.

Specimen	Advantages	Disadvantages
ENF	Widely utilized simple method	Unstable
ONF	Stable	Complex control
ELS	Stable; extended crack propagation	Variation in clamping
4ENF	Stable and simple test set-up	Limited recent experience

2.5.2 *Calculation of the strain energy release rate and R-curve according to different test set-ups*

Mode-II delamination fracture toughness refers to the resistance of a material to the propagation of a delamination (separation of layers) under shear-dominated loading conditions. Fracture mechanics states that the energy release rate, G , is the transformed energy when a material gets fractured. When the energy release rate exceeds the critical value of G_c , cracks will propagate and would be taken as a material property. It is, therefore, an important parameter in assessing the interlaminar fracture behaviour of materials like poplar plywood. Several methods and

techniques have been adopted to evaluate mode-II delamination fracture toughness, from the previously discussed tests. The most used data reduction methods are the Compliance Calibration Method (CCM), as an experimental method, the Beam theory, and the Compliance Based Beam theory.

2.5.2.1. Compliance Calibration Method

This approach is commonly used for fracture tests.

First the compliance of the specimen is calculated by the following equation:

$$C = \frac{\delta}{P} \quad (2.1)$$

Then, the Compliance is plotted with respect to the crack length: $C=f(a)$.

The obtained curve is then fitted with a first order, or a third order function, depending on the test fixture (4ENF, ELS or ENF test).

Considering the linear or the third order distribution of the Compliance/crack length function, the derived form of the compliance as respect to the crack length can be calculated and then replaced in Equation 2.2, to find the critical strain energy release rate for each crack propagation. An R-curve, which depicts the evolution of G_{IIc} as a function of the crack length can therefore be determined.

The critical strain energy release rate can be calculated from the Irwin-Kies equation:

$$G_{IIc} = \frac{P^2}{2b} \frac{dC}{da} \quad (2.2)$$

We note that, from the test configuration, we can get the necessary dimensions from the loading and crack length setup for the representations imputed in the test analysis. Also, when performing a mode II delamination test, the crack surface should coincide with the neutral axis and the cross-sectional arrangement should be symmetrical around the neutral axis in order to ensure the pure mode II fracture [18], [19].

2.5.2.2. Beam theory analysis

Although independent experiments must be performed to evaluate the Young's modulus, which varies greatly in wood, beam theory does not need crack length monitoring throughout propagation. The beam theory method is based on the deflection data of the centre of the inner span (δ) and the applied load (P). Therefore, the critical strain energy release rate can be

calculated, referring to the load and displacement data, and to the specimen's crack length and Young's modulus.

The following equation present the beam theory applied to ENF test for example:

$$G_{IIC} = \frac{9P_c^2 a^2}{16bEh^3} \quad (2.3)$$

As shown in the above equation, the fracture toughness depends on Young's modulus. Which means, that supplementary tensile tests are needed. For this reason, other analytical methods try to calculate the fracture toughness by using only the load-displacement data, such as the Compliance Based Beam Method.

2.5.2.3. Compliance based beam method (CBBM)

This method has been presented by De Moura et al. [20] and was introduced to the CCM's limitations. This technique, which was earlier established for other fracture tests, is based on beam theory, specimen compliance, and a crack equivalent calculation. It facilitates the achievement of the whole Resistance-curve (R-curve) using just data resulting from the load-displacement curve and does not need crack length monitoring. The examination of the specimen compliance while taking the beam theory into account is the first stage. The analysis starts by determining the reaction forces from the supports. Then, through determining the bending moment on each section of the specimen shown below at Figure 2.11, the strain energy due to bending effects can be provided accordingly. Therefore, the displacements at the point of loading can be determined through a derivation of ratio of stain energy versus point load at that point using Castigliano's theorem. The central point of the loading device can be determined by taking the average of displacements at the two loading points. Ultimately, the specimen compliance has been determined from the calculated central displacement and load which was also recorded continuously from the universal testing machine. As wood is a green material in which its mechanical and other properties vary drastically from specimen to specimen, the value of young's modulus must be calculated for each specimen from the expression of central displacement by imputing the initial compliance and the initial crack length. Finally, the strain energy releasing rate found with this procedure, and the R-curve ($G_{II} = f(a_e)$), can be obtained. Additionally, it is not essential to do additional experiments to determine the specimen modulus [20].

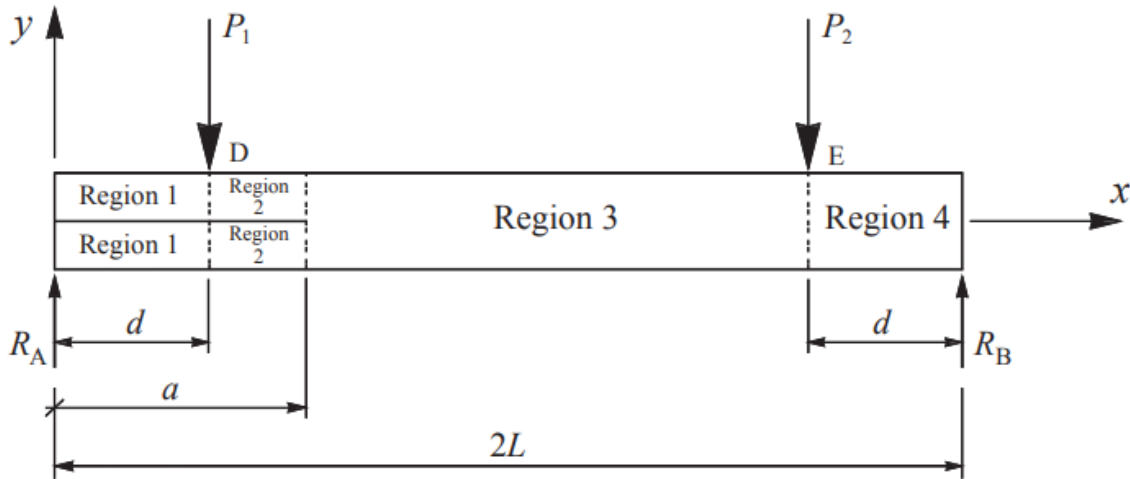


Figure 2-11: Free body diagram of the 4ENF specimen test [20].

2.5.3 Previous works on the investigation of mode-II fracture toughness of wood

Several studies have characterized the mode II delamination behaviour of solid wood. For example, Yoshihara studied the mode II fracture toughness of Sitka Spruce with ENF tests [18], [21]. Because of the crack propagation stability limits of the ENF test, the 4ENF test has been adopted by Yoshihara in other works to quantify the mode II fracture toughness of the same material [22], [23].

The specimens tested by Yoshihara were made from Sitka spruce lumber with no imperfections like knots and grain distortions. Environmental conditions were maintained and the specimens' orthotropic symmetry (having identical mechanical properties on a plane perpendicular to the longitudinal axis of the specimen) has been validated. At a first step, 4ENF tests were performed on specimens with a rectangular cross-section. However, the specimens had bending failure before any crack propagation. To overcome this uncertainty, Yoshihara has proposed a solution by making grooves along the length of the specimen aligned to its neutral axis so that an I-shaped cross-section has been adopted. As mode II is an in-plane delamination mode, there is no opening of the specimen. So, there is no clear visibility of the crack tip as it propagates. Measuring the crack length is therefore very complicated. For this reason, the crack-free portion of the specimens were labelled with lines equally spaced and perpendicular to the crack in order to monitor the length of crack propagation in accordance with loading and un-loading process of specimens which takes significantly huge amount of time per specimen (90 minutes per specimen). To compute their results of mode II fracture toughness of the tested specimens, Yoshihara used three different methods: Compliance Calibration Method, Beam theory and a

new method that he has developed: Compliance Shear Deformation method. The new CSD approach starts from determining the load-loading line compliance and the loading line displacement by the average deflection values at the two inner roller points, that have been recorded during the 4ENF test using two LVDTs at the bottom of the specimen. Once the compliance is obtained, the calculation carries on and one parameter remains unknown which is the Young's modulus of the specimen requiring a separate test. Therefore, the fracture toughness can be expressed as a function of load-loading line compliance and crack length (Figure 2.12). For the second method-CCM, separate tests have been done for specimens with different crack lengths so that the compliance-crack length relationship can be obtained by a linear regression method then fracture toughness will be calculated in order to plot the R-curve. To conclude, Yoshihara has demonstrated that the proposed CSD approach is in good agreement with CCM and beam theory, and its advantage is that no separate test is needed to obtain the R-curve. However, this approach may need a complicated arrangement of the LVDTs on the back of the specimen, that are essential to measure the longitudinal strain at points below the specimen.

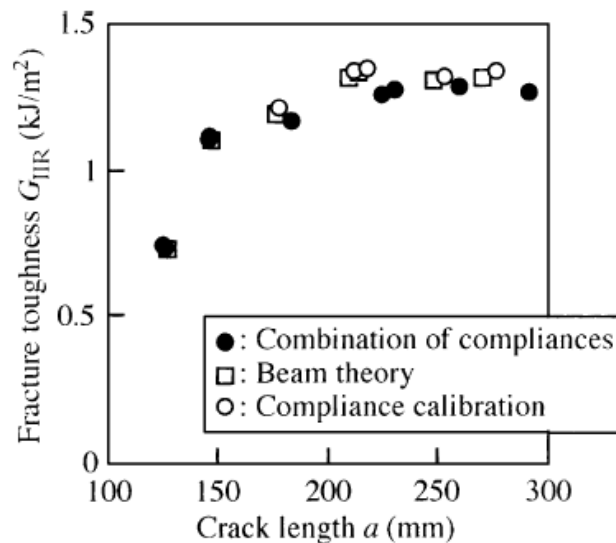


Figure 2-12: Calculation of the fracture toughness of solid wood by the three methods proposed by Yoshihara [22].

The fracture behavior of wood under mode II stress was also thoroughly examined by De Moura et al. [20], along with an appropriate data reduction strategy and a finite element analysis validation. To characterize the behavior of Pinus Pinaster wood specimens under mode II loading, the Four-Point End-Notched Flexure (4ENF) test has been used. Similarly to Yoshihara's test procedure [22], De Moura et al. have adopted the I-shaped cross section for their specimens, and load/unload cycles during the 4ENF test. The Compliance based beam

method (CBBM), which uses data reduction from the load-displacement curve was used to compute the R-curves for the tested specimens, as depicted in Figure 2.13. To overcome the need of Young's modulus value to calculate the strain energy release rate with the CBBM, De Moura et al. [20] have proposed to calculate it from the initial compliance and the initial crack before crack propagation. With this solution, the authors have needed only data from load-displacement curve to calculate the fracture toughness of the specimens, without any need to further tensile tests to extract Young's modulus. De Moura et al. [20] have also validated their experimental results with a method based on beam theory and also with the results of numerical modelling based on the cohesive zone model.

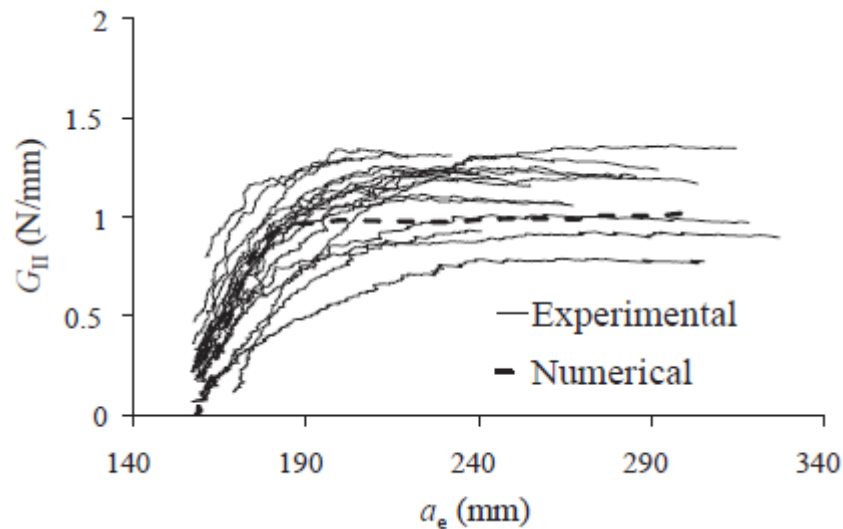


Figure 2-13: R-curves obtained by De Moura et al. for *Pinus pinaster* wood specimens [20].

While many studies have focused on determining the fracture toughness of solid wood, very few have studied that of LVL or plywood. Franke et al. [24] have interested in quantifying the interlaminar fracture toughness under Mode I and II and the mixed mode loading of New Zealand Radiata Pine timber and Radiata Pine LVL. They have concluded that Radiata Pine LVL is more ductile than Radiata Pine timber, leading to a lower mode II fracture toughness for LVL than for timber. Interested to plywood failure behaviour, El Moustaphaoui et al. [25]–[27] have characterized the mode I and II and mixed mode fracture toughness of the interface between two plies in the direction of the *Ceiba* wood fibres (0° direction). For mode II particularly, El Moustaphaoui et al. [25]–[27] chose the ELS test for their *Ceiba* plywood specimens. To find the R-curve without need to monitor the crack length experimentally, they have referred to the beam theory using the load and displacement from 4ENF test data and longitudinal Young's modulus from tensile tests. Between all the studied modes, They have concluded that the energy required for delamination under mode II loading was higher than that for mode I or mixed mode. By investigating the fracture surfaces interface of the specimens

after failure, El Moustaphaoui et al. [25]–[27] have highlighted the significant presence of fibre bridging and crack tip splitting for mode I and mixed mode specimens. But those phenomena were absent for ELS specimens under mode II loading.

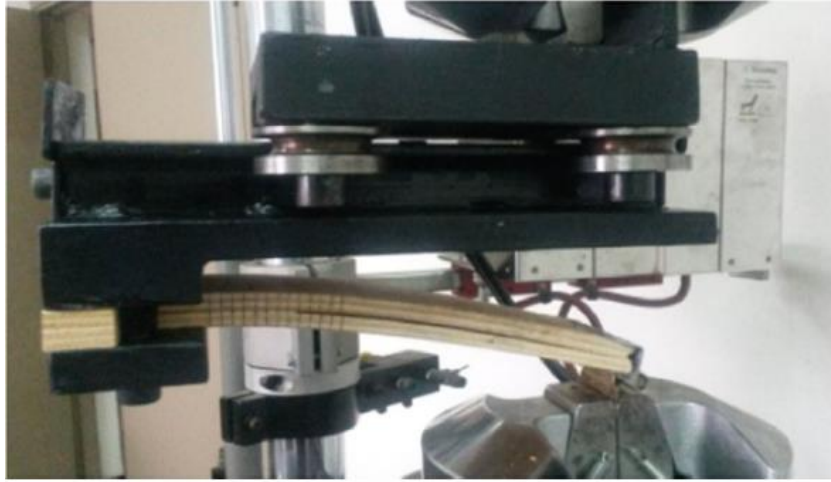


Figure 2-14: Geometric ELS test fixture adopted by El Moutaphaoui et al. [27].

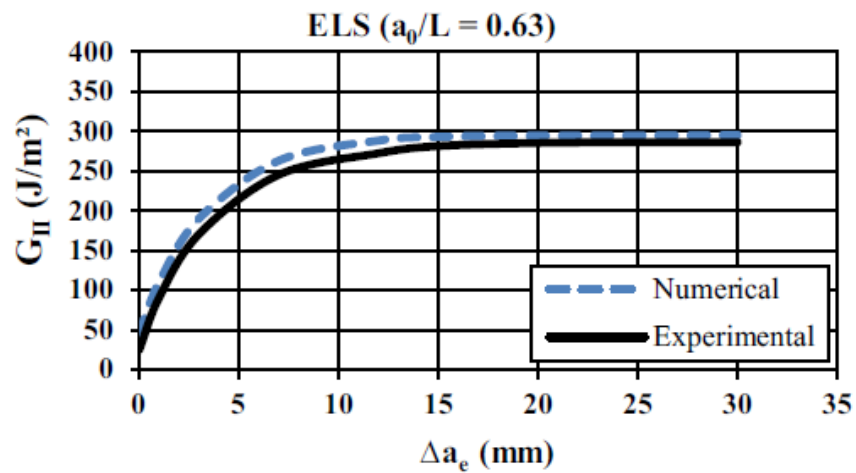


Figure 2-15: R-curves obtained by El Moutaphaoui et al. [27] using ELS test for plywood specimens.

In all the above cited works, the mode II interlaminar fracture toughness was found by considering a $0^\circ/0^\circ$ interface only, and without a continuous crack tracking during the test. Plywood is, by definition, composed of cross-ply veneers perpendicular to one another. So, it is important to determine the mode II fracture toughness of plywood with $0^\circ/0^\circ$ but also $0^\circ/90^\circ$ interface.

In this context, we propose in this work a characterization of the mode II interlaminar fracture toughness of poplar plywood with $0^\circ/0^\circ$ and $0^\circ/90^\circ$ interfaces, using 4ENF tests.

2.6 Conclusion

Ultimately, through reviewing various previous works and understanding the big picture of the procedures they followed on the characterization of wood, different test setups were discussed accordingly, while most of the approaches were conventional on the extraction of important data like crack propagation, strain, and displacement as the task deals with a material with a non-uniform mechanical property throughout its axis. Therefore, the insight of this paper runs to explain how those parameters have been attained through adoption of a unique system in the data acquisition to run the experimental and analytical calculations. This work selects the 4-ENF test method as it has stable crack propagation and has been giving better results relatively.

THIS PAGE WAS INTENTIONALLY LEFT BLANK

3. MATERIALS AND METHODS

3.1 Introduction

Through a thorough study of identifying the most intricate behaviour of a wood material, several factors are accountable for that varying performance on the application area. The major difference lands in Macro and Micro structural behaviour within the material, plywood in this work.

Apart from the inherent behaviour of plywood, a high attention must also be given to the proper design and manufacturing of specimens to be tested in the process of identifying mode II fracture toughness: critical energy release rate.

3.2 Specimen design and manufacturing

In this section, we will discuss the size and design of the specimens used with their orientations of fibres at the plies followed by their manufacturing process and preparation for the test.

The aim of this work is to characterize the mode II interlaminar fracture toughness of plywood and to analyse the influence of changing the fibre orientation at the interface on the fracture behaviour. To do that, specimens made of poplar plywood and with two configurations of fibre orientation in the interface: $0^\circ/0^\circ$ and $0^\circ/90^\circ$ are manufactured and tested (Figure 3.1 and 3.2). For the specimens having crack interface between $0^\circ/0^\circ$ plies, the crack propagation is expected through the adhesive joint or at the interface between the wood and the adhesive. The second fibre orientation, $0^\circ/90^\circ$, is expected to have crack path through the 90° fibres.

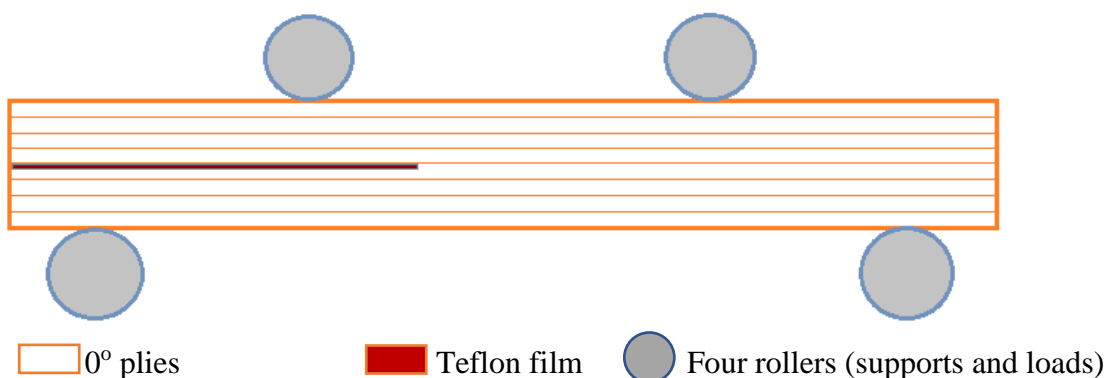


Figure 3-1: $0^\circ/0^\circ$ Specimen

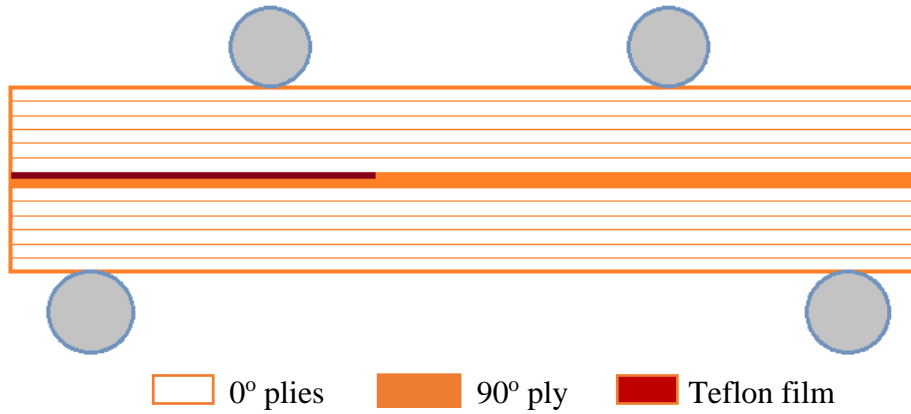


Figure 3-2: 0°/90° Specimen

3.2.1 Dimensions of specimens

As there were no processing guidelines or standard for preparation of laminated plywood panels for the assessment of mode-II fracture toughness especially for the 4ENF test, the dimensions of the specimen can be determined by taking the average value from previous similar studies and referring standard for unidirectional carbon fibre composites. For instance, the standard ASTM D7905-14 as a reference, gives a specimen length more than 150mm and width in the range between 20-30mm [11]. From the literatures (Yoshihara et al. [22] and De Moura et al. [20]), tests have been conducted with a specimen length of 500mm (longitudinal direction). In this work, specimens have a length of 250 mm and a width of 25 mm (Figure 3.3). Preliminary test have been conducted for both fibre configurations with 8 mm of thickness of specimens and bending failure before crack propagation was a barrier for the 0/90 plywood specimens. Therefore, to overcome this uncertainty, the bending stiffness of those specimens could be enhanced by increasing their thickness through adding up more plies than the 0/0 specimens. Through this technique, enough shear load can be concentrated on the interface to initiate crack. So, the 0/0 specimens have thickness of 8 mm with 8 number of plies on the contrary the 0/90 specimens have thickness of 13 mm with 13 number of plies.

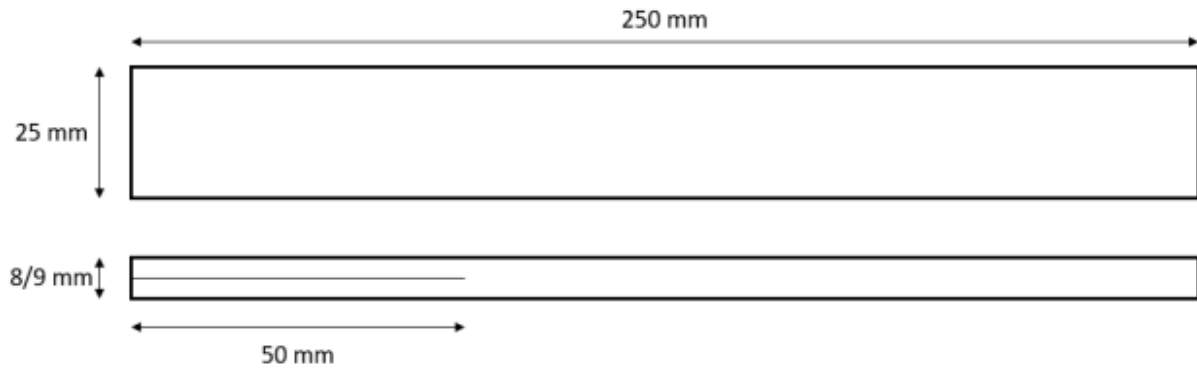


Figure 3-3: 4ENF specimen dimensions

3.2.2 Manufacturing process of plywood plates

Poplar plywood plates were manufactured by pressing glued poplar veneers for 5 hours at 10 bars and 25°C. The poplar veneers were supplied by the LaBoMaP laboratory in Cluny, France, with a thickness of 1 mm and a density of 348 kg/m³. The manufacturing process is therefore divided in two parts: the manufacturing of the poplar veneers (at LaBoMap), and the manufacturing of poplar plywood plies at ICA. The whole production process is described in the following steps (Figure 3.4):

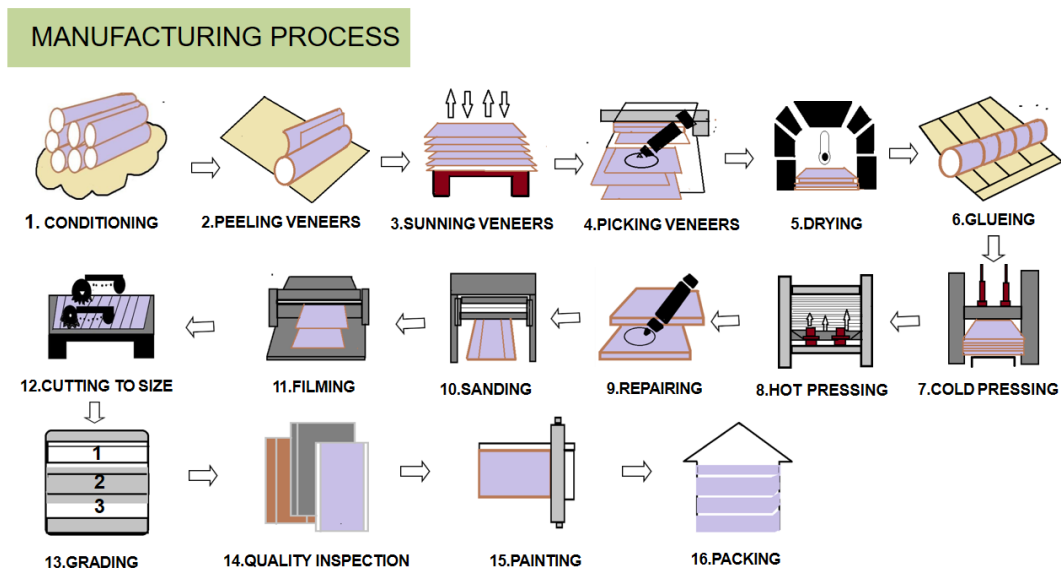


Figure 3-4: Overall manufacturing process of plywood [28].

Step-1: Choosing high-quality poplar logs is the first stage in the making of plywood. For the procedure, logs with an appropriate diameter and no flaws must be picked [28].

Step-2: Debarking and cutting: After the logs have been chosen, the outer bark covering is stripped off. The logs are then chopped into more manageable lengths for further processing after being debarked [28].

Step-3: Peeling: Poplar wood is produced by rotating the logs against a sharp blade to create thin layers or veneers using a rotary wood peeling machine (Figure 3.5). These veneers serve as plywood's basic building components. The veneers supposedly have a thickness of 1mm provided by a research laboratory named “LaBoMaP” located at Cluny in France. The laboratory has been involved as this work is part of the ANR BOOST project.

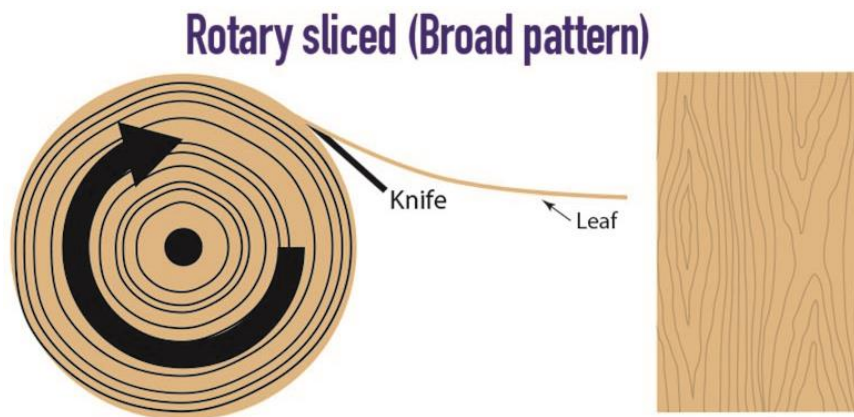


Figure 3-5: Peeling operation [28].

Step-4: Grading and sizing: the veneer is sized to a standard 600mm×630mm as shown in the figure 3.6. It is known that this natural material has strange mechanical properties the fact that it has a non-uniform microstructure and distribution of fibers, therefore it is viable to propose naming of veneers due to their variation. After the peeling process has been done, the unrolling of the veneers induces a significant number of small cracks on one of its faces which would cause a major factor for their difference in performance while conducting the test. Therefore, numbering of this face is necessary to better understand the characteristics of the specimen during the test. The veneer numbering process is presented in Figure 3.6.

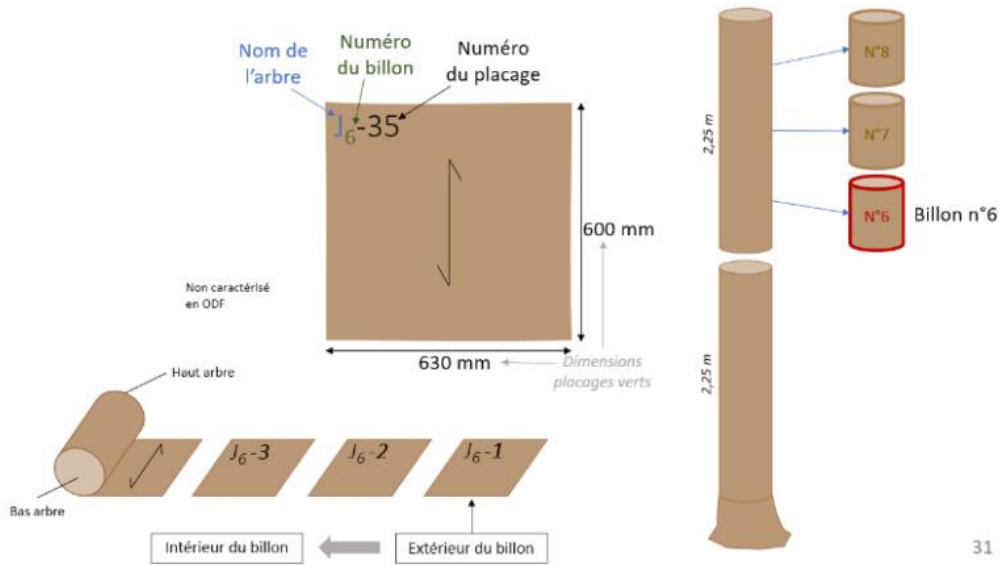


Figure 3-6: Veneer numbering (ENSAM Cluny, France)

Step-5: The poplar veneers are now ready for gluing. This step was realized at the ICA, Toulouse. The veneers are attached to one another using adhesive, which is often a sort of resin or synthetic glue called polyurethane wood glue with a density of 250g/m^2 . Glue application is done using a 60ml syringe to apply 80ml glue through two strokes. The nozzle part of the glue has to be cut as the viscosity of the glue is high and the flow would be facilitated. Then, a uniform distribution of the glue is done using a spatula (Figure 3.7). The wood layers are firmly bonded to one another due to the proper gluing procedure. The two series of specimens, 0/0 and 0/90, with 8 plies of 0-degree fiber orientation and 13 plies: 12 plies of 0-degree and 1 ply of 90-degree, are finally manufactured.



Figure 3-7: Glue Application on the veneers

Step-6: Pressing:

Cold Pressing: After the introduction of glue through the plies, release film and rip cloth are applied to the plywood plate (Figure. 3.8), to prevent the glue from adhering to the steel plates of the press machine. After positioning the plywood plate between the steel plates of the press machine, 10 bars of pressure is applied to the plywood plate within a hydraulic press for 5 hours

at an ambient temperature of 25°C. The pressing procedure starts by quick engagement of the upper press jaw up to 20cm then gentle closeness of the jaw for 20min until the 10-bar load is applied. Finally, the load will be maintained for the duration of 5 hours and then it will be disengaged, taking 10 minutes (Figure 3.9). The applied amount of pressure ensures a homogeneous distribution of the glue and a stronger adhesion between the pressed plies.



Figure 3-8: Plies inside the press machine ready to be pressed.



Figure 3-9: Press machine

Two plates were manufactured at ICA, Toulouse, according to the pressing procedures described above: 1 plate with an interfacial fiber orientation: 0°/0° and 8 plies oriented at 0° stacked into the press machine, and one plate with an interfacial fiber orientation 0°/90° with 13 plies: 12 plies at 0° and 1 ply at 90°. As the operation of cutting out specimens out of the pressed plates needs special machine and equipment, it has been carried out in Tarbes at

National School of Engineers of Tarbes-ENIT. We note that 16 specimens were cut from the $0^{\circ}/0^{\circ}$ plywood plate, and 17 specimens were cut from the $0^{\circ}/90^{\circ}$ plate.

3.2.3 *Formation of pre-crack*

In order to concentrate the effect of the load on the intended interface area to study mode-II delamination, there must be an intentional notch or crack on the specimen. Therefore, the study will be held starting from the end of the pre-crack of the specimen. The formation of the pre-crack will take place at the time of gluing of the plywood plies by using Teflon tape placing it in between the plies where the pre-crack needs to be placed as that area would be a glue-free area. Three pieces of tape were placed over a length of about 14cm. Also, a cutter was used to remove the inflowed and dried portion of the glue in the pre-crack region.

3.2.4 *Cutting out the specimens*

As the operation of cutting out specimens out of the pressed plate needs special machine and equipment, it has been carried out in Tarbes at National School of Engineers of Tarbes-ENIT. Illustration of arrangement of specimen layout on the plan of the plate shown below (Figure. 3.10). the press cycle would be four times as we have 33 specimens, 16 for the $0/0$ and 17 for the $0/90$ and according to their dimensions in relative to the dimension of the plate, maximum of 10 specimens can be cut out of it. The specimens are positioned in the veneers as shown, leaving the appropriate space for the press and laser cutting. Illustration of arrangement of specimen layout on the plan of the plate shown below (Figure. 3.10 and 3.11).

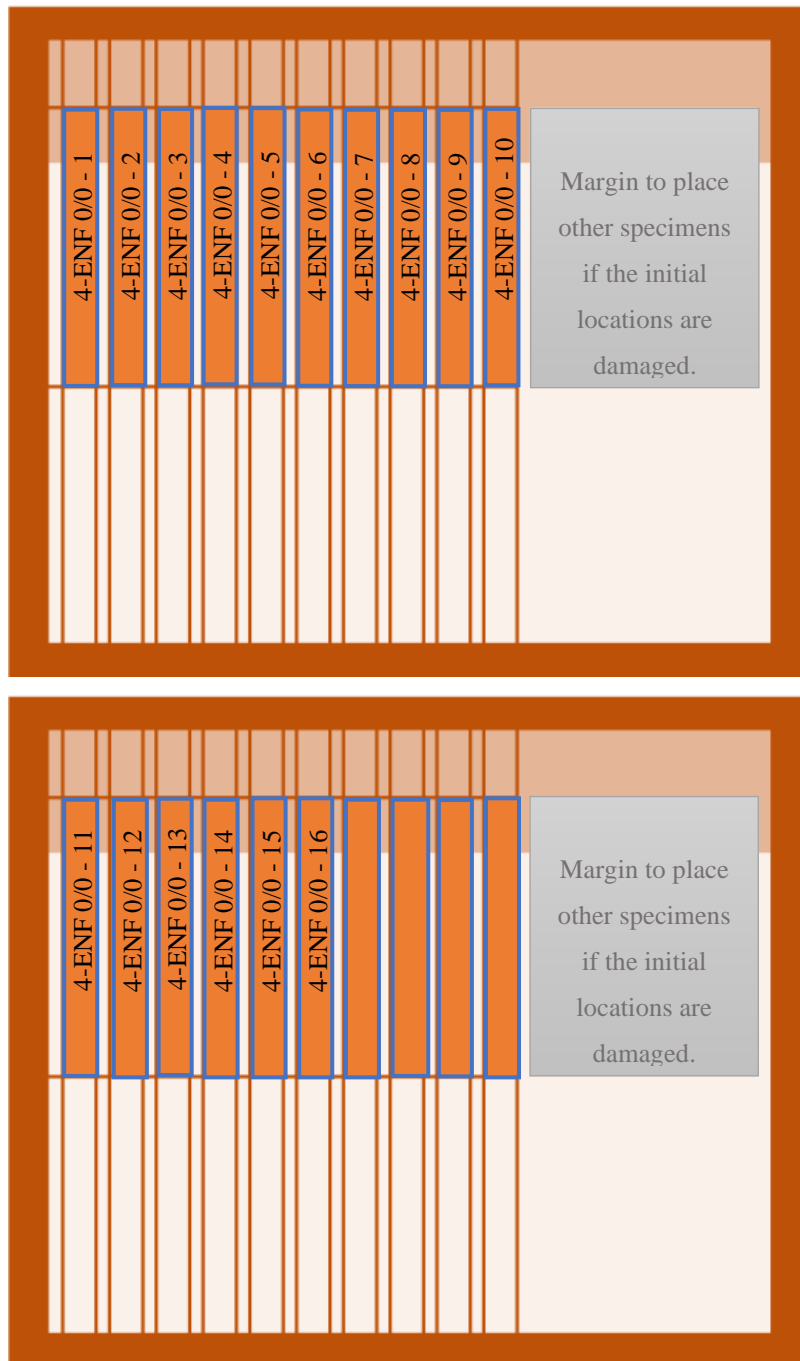


Figure 3-10: Arrangement of 0°/0° specimens in veneers plate.

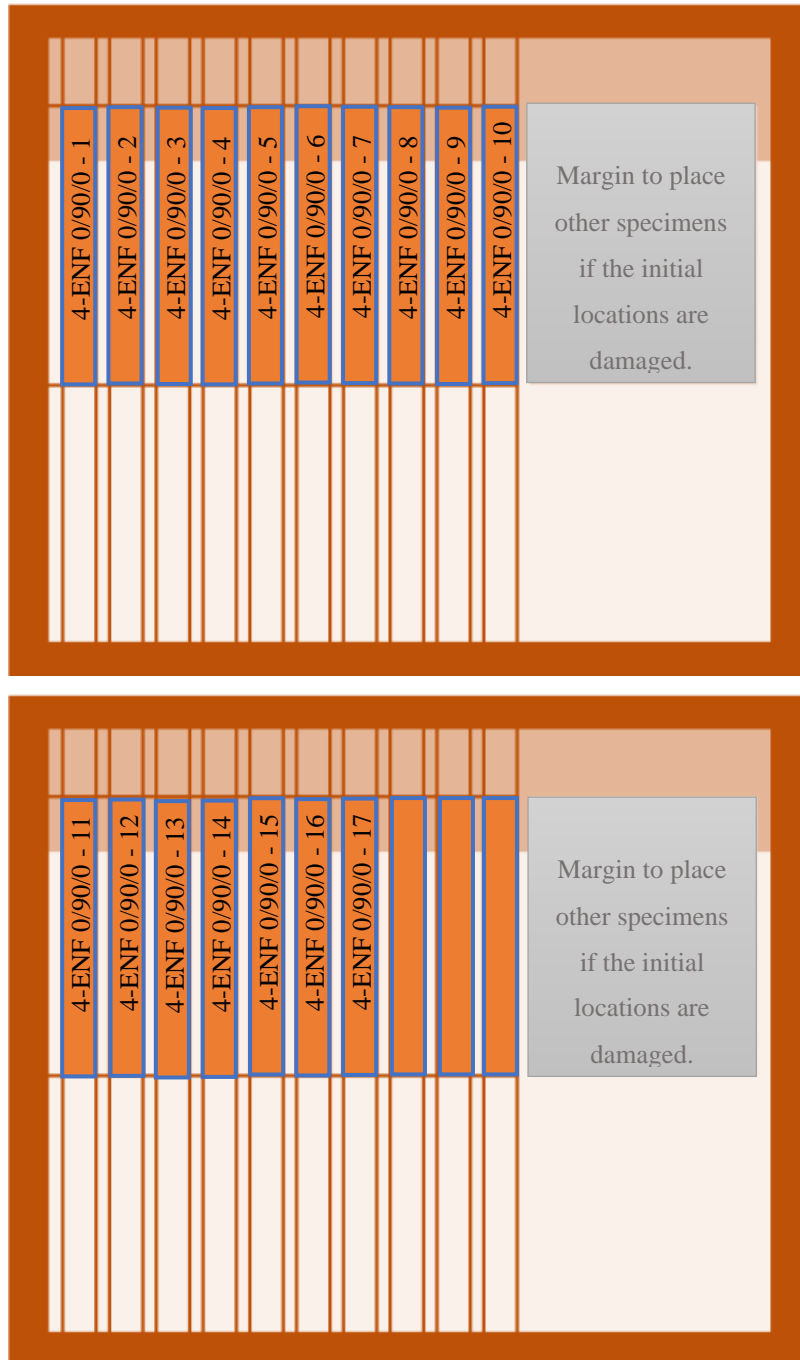


Figure 3-11: Arrangement of 0/90/0 specimens in veneers plate.

The specimens are cut in accordance with the configuration shown above. Ultimately, 33 samples were taken. With the help of 8 extra samples, conducting a pre-liminary test would be feasible to gather more information and evaluate the testing procedures before beginning.

3.2.5 Preparation of the specimens for the 4ENF test

It is required to paint one of the thickness sections of the specimen in order to get it ready for data gathering techniques. In fact, the stereo-correlation of the images and infrared acquisition

will be employed on one side of the specimen. For the stereo-correlation of images, a speckled surface needs to be created on that side. For this reason, the specimens are first painted in white. When the white paint is completely dry, a matt black spray should be used to speckle the surface while keeping a reasonable distance from the test specimens (Figure 3.12). Only tiny paint droplets are applied to the test specimens in this manner, yielding a typical speckle having an appropriate size for the focal depth of the DIC (Digital Image Correlation) cameras. Indeed, the size of one speckle is approximated to 0.12 mm, which correspond to a minimum size of 3 pixels, as recommended by Reu [29] (Figure 3.13). The white painting permits a clear contrast with the black speckles.

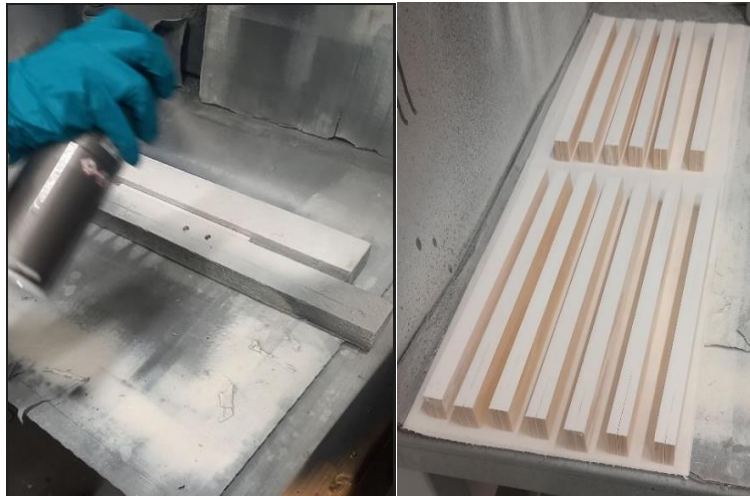


Figure 3-12: Spraying of specimens.

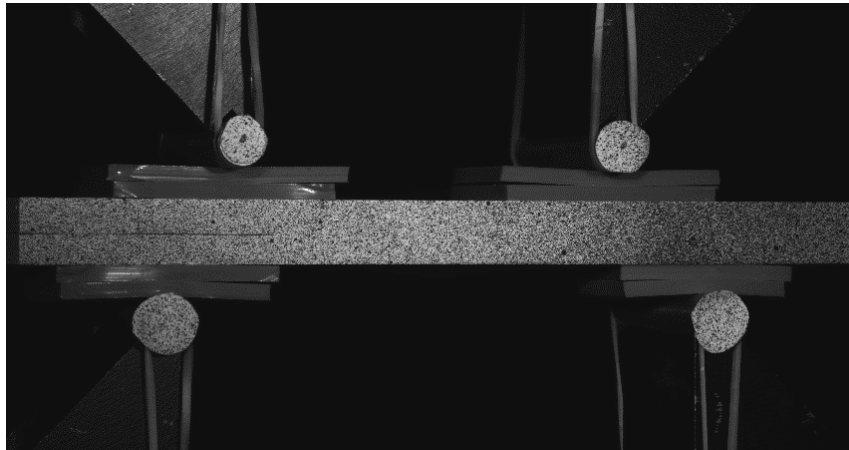


Figure 3-13: Speckles on the specimen and faces of rollers.

3.3 Four-point end notch flexure test set-up

From the adoption of preferred test configurations through reviewing previous test procedures and works, 4ENF test method has appealing feature in terms characterization of materials determining mode-II delamination behaviour. Tests of manufactured 33 specimens were carried out in April 2023 at the Mechanics of Structures and Materials Department (DMSM) of National School of Aeronautics and Space (ISAE-SUPAERO). The test campaign took 3 days for setting-up the test, calibrating the cameras, and realizing the tests.

3.3.1 Test equipment

A successful material testing highly rely on a well-coordinated manner of testing equipment. Factors such as, position of equipment, calibration method, condition of testing room, level of parallax error, and proper follow-up of test procedures really matter on the investigation of mechanical property of a material. Below, discussion of different equipment used will be presented in accordance with their set-up.

3.3.1.1 50kN Universal Testing Machine

As the Universal testing machine has a versatile feature to conduct different types of tests, modification of test configuration has been manipulated bringing 4-ENF test set-up. The machine used was the INSTRON 5900.



Figure 3-14: 5900 series universal testing systems-Instron.

It was a challenge to fix the assembly of loading and support rollers to keep proper bending load on the specimen (Figure 3.15). Conventional pivot joint (Figure 3.16) has been adopted between the load cell loading point and the horizontal loading arm. This is because our material is naturally non-homogenous and has a non-uniform bending stiffness along its major axis,

specifically longitudinal axis. Therefore, balanced average bending load must be applied all along the length of the specimen. Maintaining that can be achieved by proposing a special pivot that controls the amount of bending load exerted on the specimen. So that average deflection would be taken for the analysis ahead from the effect of the applied load which is not distorted by the non-linear behavior of the specimen, plywood laminate.



Figure 3-15: Experimental setup of a four-point bending test

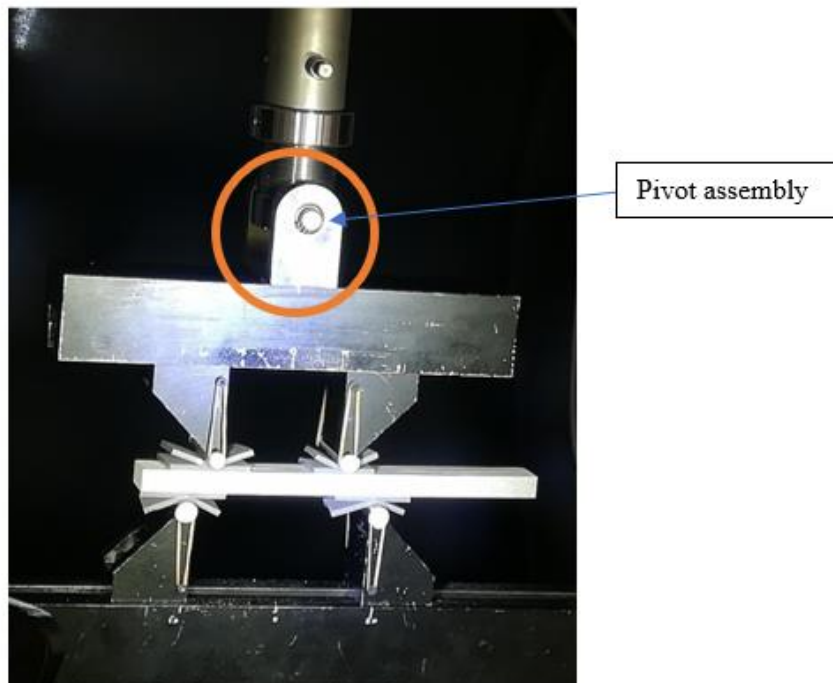


Figure 3-16: Test set-up assembly with the specimen

3.3.1.2 Digital image correlation device

Cameras and speckle patterns are used in the optical 3D deformation measuring technology known as digital image correlation (DIC), which provides full-field strain and displacement data. Its correctness is checked against established techniques. With stereo camera configurations for 3D measurements, it provides versatility and speed when used in structural and member deformation measurement. It uses speckle patterns to monitor strain and non-contact deformation. It functions at ranges ranging from micro to macro and is effective for many different applications, including field inspections. The effectiveness of DIC has been shown in 2D and 3D deformation analysis, following changes in the speckle pattern for strain/displacement data. DIC, an optical 2D measuring method, depends on image tracking and registration for accurate findings. Strain and displacement are calculated using correlation coefficients from pixel intensity arrays (Figure 3.17).

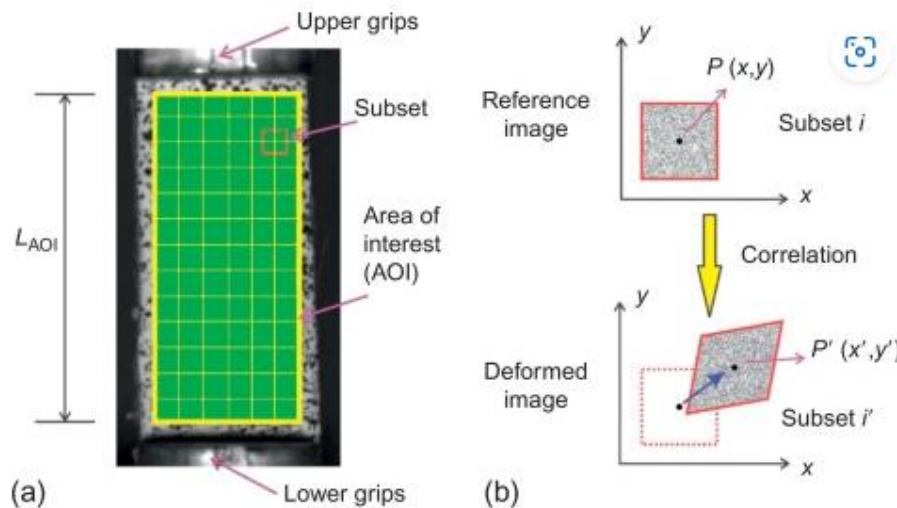


Figure 3-17: (a) Area of interest (AOI) and subset in a reference image; (b) schematic presentation of a reference subset before deformation and the corresponding target subset after deformation [30].

DIC is one of the key techniques for material characterization using dual camera chambers tracking and measure the distance that the speckles move between photos as the specimen deflects on the continuous loading effect which causes crack propagation under mode-II delamination [30]. The set up consists of two cameras and a light spot. The specimen is in front of the first camera. The second is slightly out of alignment, in this case by an angle of around 8° . The image acquisition software VIC (Volumetric Image Correlation) Snap is connected to the cameras. After that, the data is exported for VIC-3D processing. Calibration would be done using a reference plate or a calibration chart having black spots and then the cameras would take different shots tilting the plate in different angles and directions relative to the specimen

ready to be tested (Figure 3.18). This helps the software to detect and analyze the movement of the speckles on the specimen precisely.

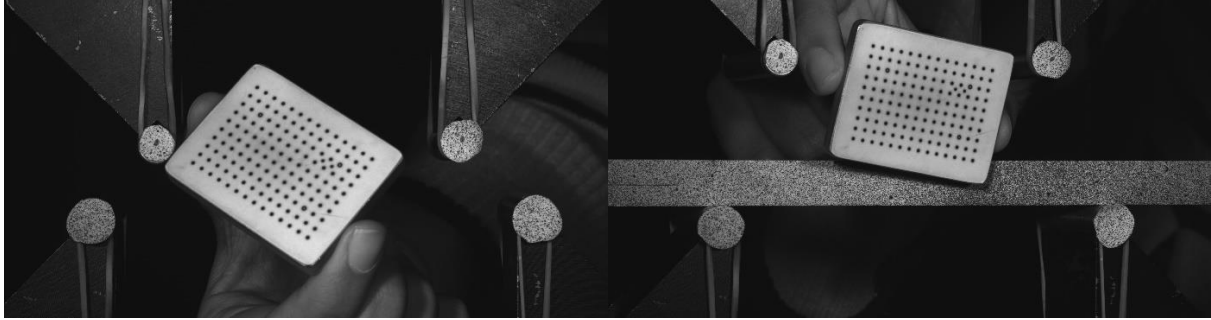


Figure 3-18: Calibration process

3.3.1.3 Infrared thermography device

Due to its capability to non-destructively evaluate the interior structure and state of materials, an Infrared (IR) thermography instrument is essential for material testing (Figure 3.19). It generates thermal pictures that show temperature gradients and abnormalities inside the material by detecting differences in infrared light produced by the item. All sources of heat and light must be kept to a minimum so that observation may be done as effectively as possible. A blackout panel has been set up facing the camera for this purpose. This is accomplished by draping a protective panel in many layers of black cloth. The field of the camera must be kept clear of any computers or displays that produce heat.

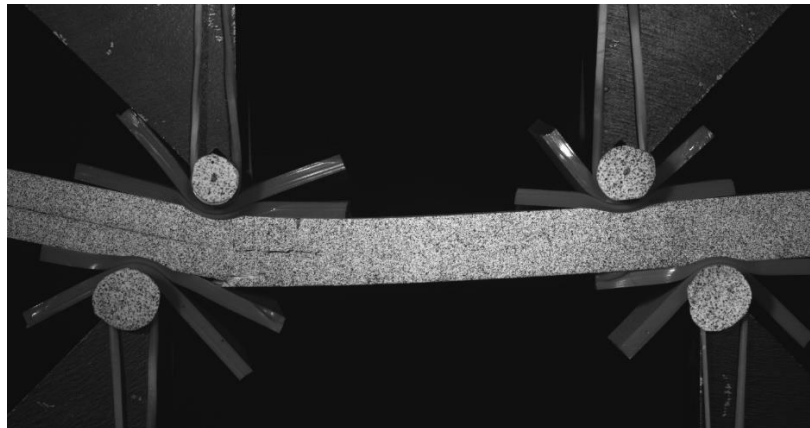


Figure 3-19: Infrared thermography device and Dual camera setup with a blackout panel as a background of the specimen.

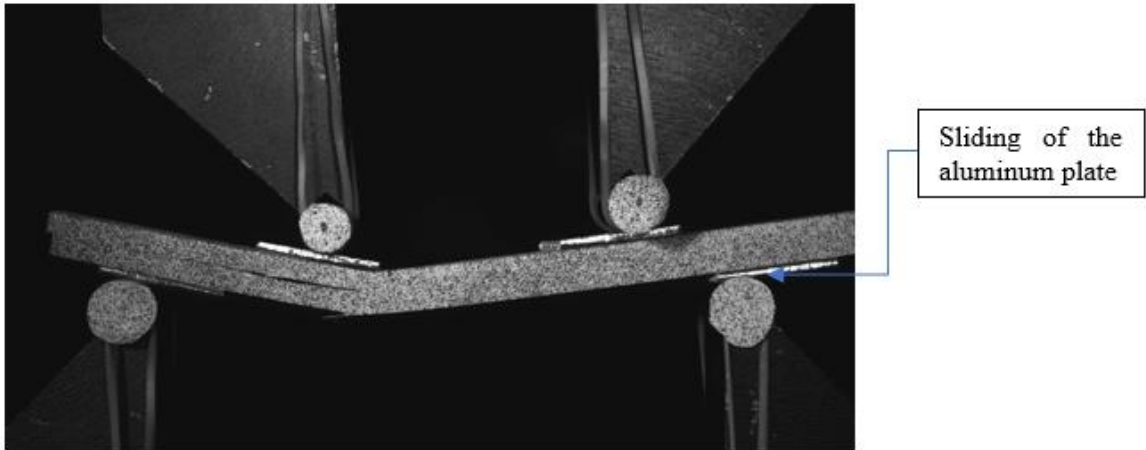
3.3.2 Test set up and procedures

Implementation of organized test procedure is important to have a consistent data and results of each test which will be a governing basis for each specimen.

With preliminary tests conducted on some specimens, we have remarked that there is marking of the rollers on the specimen surface, which refers to the squashing of wood at the contact with the rollers. In order to overcome this issue, inserts of Aluminium plates and silicon pads have been tried in between the specimen and the rollers (Figure 3.20). While the specimen is bending, the loading rollers were rotating on the aluminium plate. This results in sliding of the aluminium plate, out of the specimen fixture, which makes it unideal to continue the test. The silicon pads have been good in terms of distributing the load and not marking the local area under the rollers. The specimens positioned on the 4ENF fixture, with silicone pad at the contact with the rollers, is finally ready to begin the test. We note that the image acquisition from the cameras were started same time as the beginning of the test, to make sure that the recording images and the applied load/displacement are synchronised. The test and the image recording are stopped when the specimen is fractured.



(a) Test with silicon pads as an insert



(b) Test with aluminium plates as an insert

Figure 3-20: Launching of the pre-liminary test.

3.4 Post-processing of experimental data

The machine provides information on the reaction force by the specimen registered on the load cell and the displacement of the machine while bending the specimen at each instant. Regarding infrared thermography and stereo-correlation, the data provided are images. There is therefore a lot of post-processing work to be done. Below, the detailed data processing scenario is presented.

3.4.1 VIC-3D calculations

Here the detailed steps on the VIC-3D software will be presented. After importing the calibration and speckle images, the score of calibration must be calculated for the software taking that parameter to continue with the speckle images and detecting them. The score must be below 0.03 in order to say the calibration is optimum for the calculation and analysis within the software (Figure 3.21).

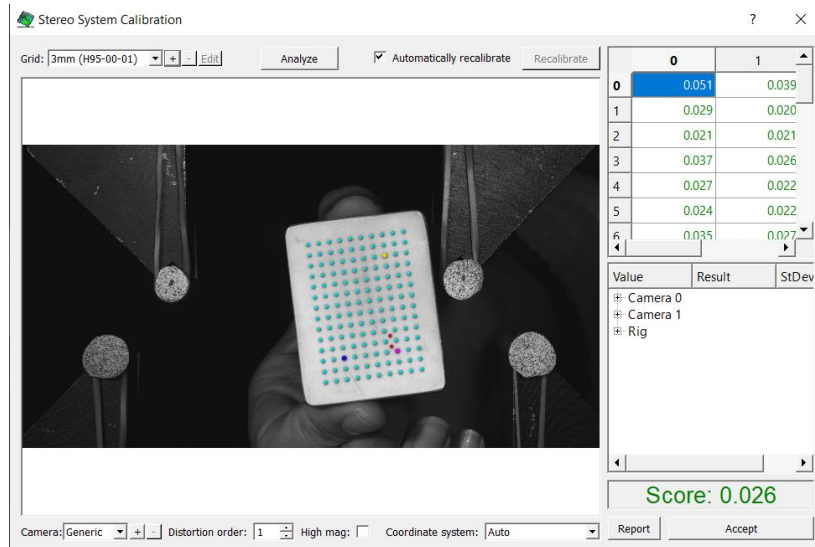


Figure 3-21: Stereo system calibration

The following step is selecting a region for image-correlation analysis on VIC-3D and selecting a start point for the calculation where the displacement of the specimen is the weakest close to the loading roller at the uncracked part of the specimen (Figure 3.22).

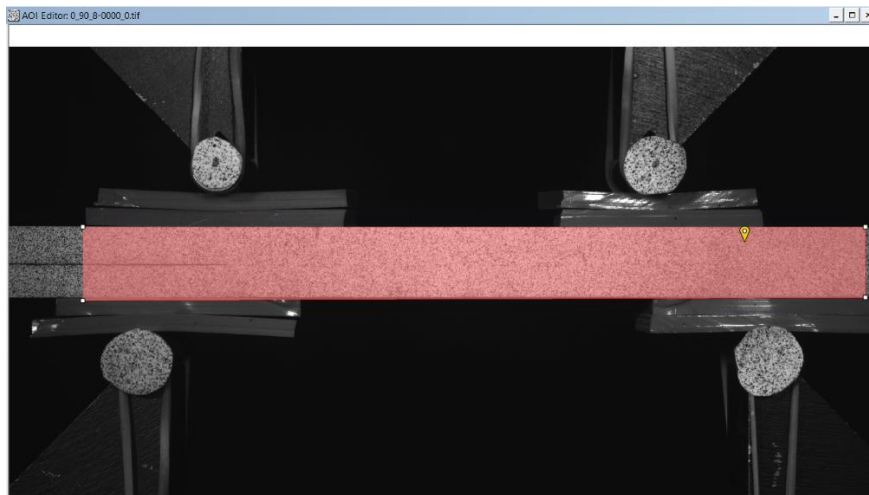


Figure 3-22: Region for the analysis and start point.

After selecting the region, the area must be divided into many small square of calculation as it is called subsets. The more refined subset ensures more precise calculation on the software. Therefore, the subset size is determined considering the optimum number of speckles inside a single subset as the system co-relates the movement of the speckles in each image. Therefore, a number of 3 to 4 speckles per subset is chosen (Figure 3.23).

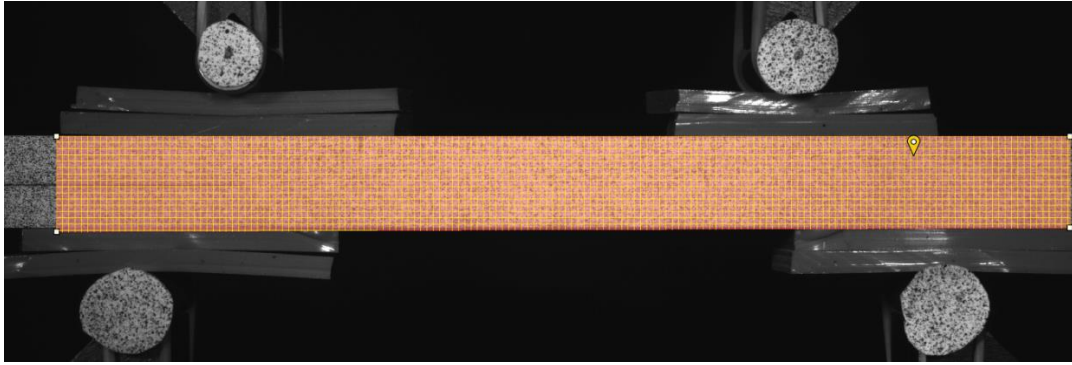


Figure 3-23: Meshing the region with respect to subset and step parameters.

The threshold parameters are also modified. The different parameters chosen are presented in Figure 3.24.

Then the analysis would run after setting up those previous parameters. The analysis running time takes an average of 15minutes per specimen to process the 150-300 images recorded during a test (Figure 3.25).

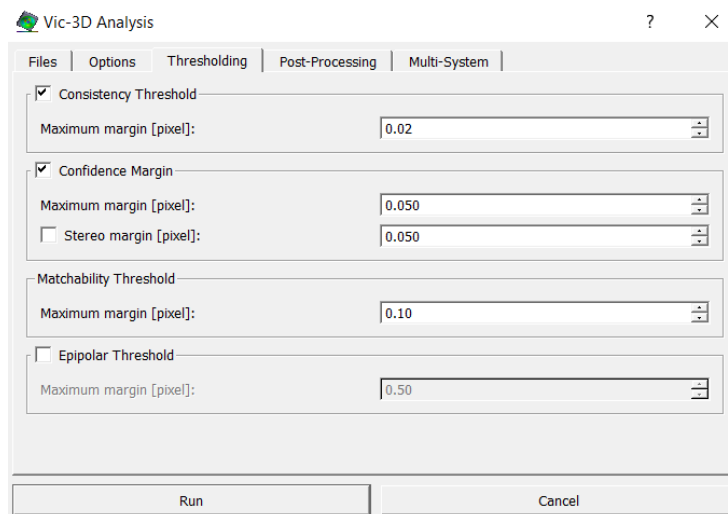


Figure 3-24: Threshold settings

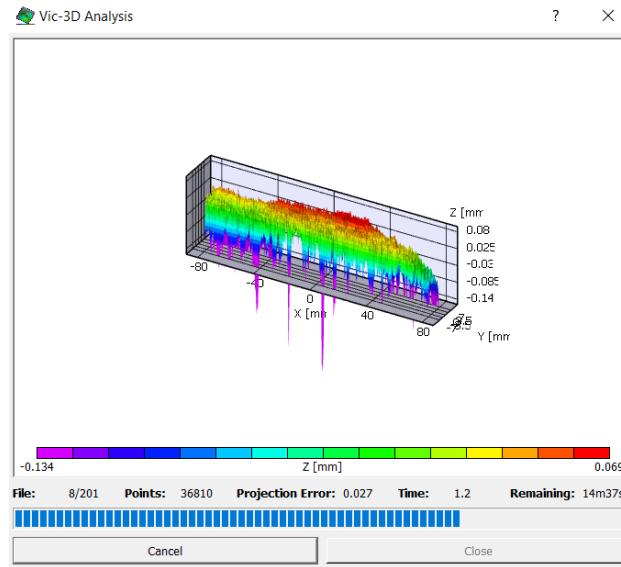


Figure 3-25: VIC-3D Analysis in progress

3.4.2 Curves of the force-displacement

As stated above, the machine keeps registering the load and displacement during the test. And from this data, the plot can be displayed on the computer from the data acquisition system. Supposedly, the displacement which was taken from the machine was considered as the theoretical exact deflection of the specimen. But the silicon insert has an influence on the force-displacement data as it has some value of resisting force registered on the load cell of the machine and values of deflection as well which is not part of the specimen. Ultimately, the excel data distribution of force-displacement is not going to be considered for the calculation of strain energy releasing rate unless the true displacement of the specimen is extracted corresponding to its load value. The solution for this issue would be taking the displacement information from the images which has been taken and used under the image-correlation technique inside VIC-2D/3D software. After selecting the region of the specimen on the software, four inspection points were placed on it near to the four rollers, as shown in figure 3.26.

Then the software relates every taken images and extracts the plot for the vertical deflection of these four points. Finally, the average of these values of deflection would be calculated and that being the true deflection of the specimen for the analysis (Figure 3.27).

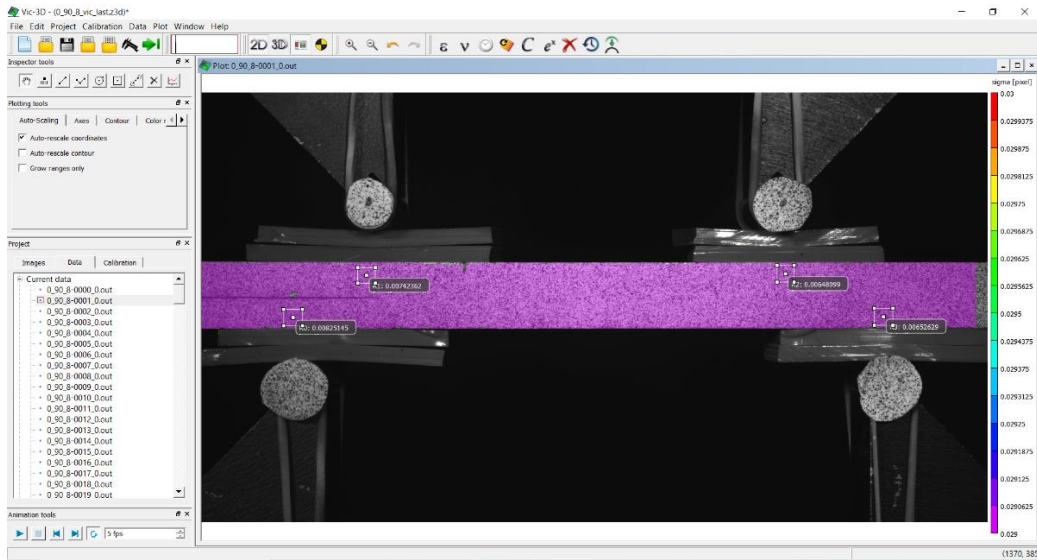


Figure 3-26: Displacement points on the specimen



Figure 3-27: Displacement extraction plot

3.4.3 Crack propagation calculation

What makes this project different from previous works on plywood is the method adopted to monitor the crack propagation. The DIC technique is used in order to track the crack as it propagates by referring to the recorded images from 4ENF test. VIC-3D was used to generate a progressive video of all the recorded images, which is then imputed into a python script to track each crack progression per image of the specimen and a txt file of the coordinates of the crack tip is generated. Those coordinates are then used to calculate the crack length for each image.

To see clearly the crack tip on the recorded images, we refer to the parameter “sigma” on Vic-3D. This parameter represents the correlation error between the images recorded during the test (images where we have a crack propagation), and a reference image, which is the first image

taken at the beginning of the test. Sigma equal to 0 indicates a perfect match. Higher values of sigma indicates that there is a large difference between the two images, which may refer to a crack propagation.

First, the noise in the study area in the reference image (Figure 3.28) is removed by eliminating the small values of sigma. This enables a clearer display of the crack bottom after each propagation, which corresponds to high values of sigma, as depicted in Figure 3.29.

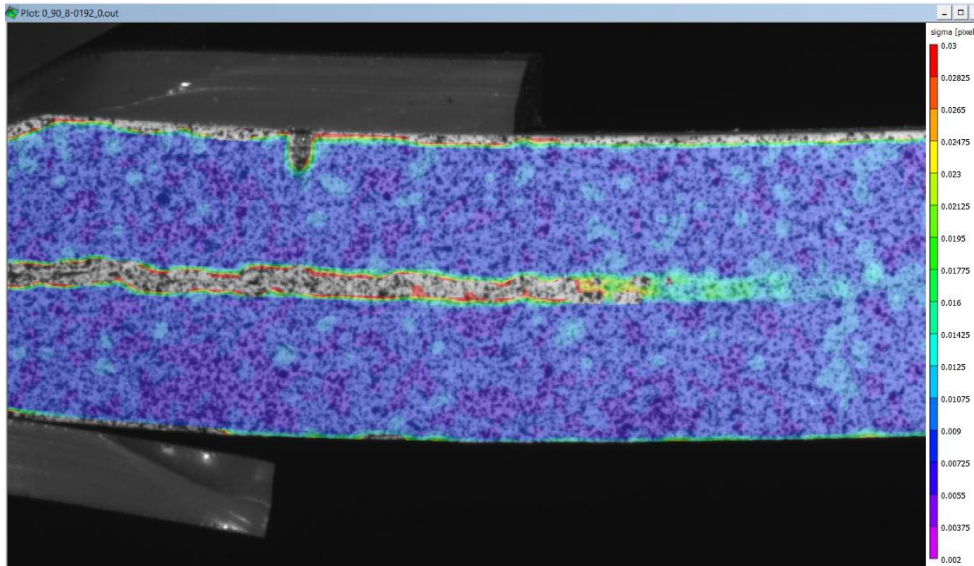


Figure 3-28: Crack propagation with noise

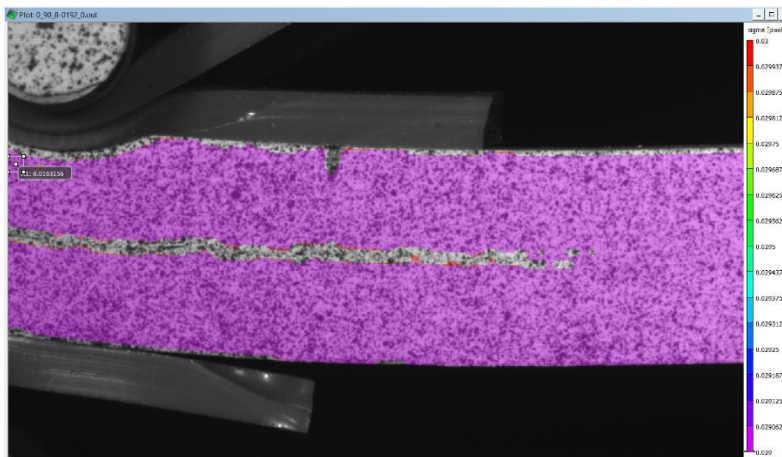


Figure 3-29: Sigma value adjustment for a clear crack tip

After having clear crack tip and path, the next task would be exporting all the analyzed shot images to a video format (Figure 3.30) in order to impute it for the python script which used to do the tracking of the crack tip.

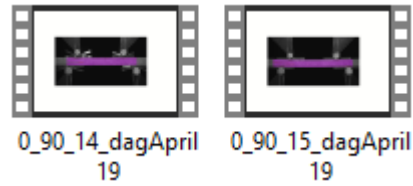


Figure 3-30: Example of videos extracted from VIC-3D software

The provided python script has a library module called moviepy which helps to track each progression of crack tip corresponding to each image (Figure 3.31). The library module has a function called *Manual Tracking*, which is done by clicking every crack tip until the specimen reaches up to failure. Therefore, all the point by point clicked positions are registered in pixels and saved as a txt file format. Those values of pixels must be converted to millimeters through determining a scale. The position of outside rollers in pixels is $x=467$; $y=503$ and $x=1027$; $y=498$ left and right respectively (Figure 3.32). The pre-crack length is 40mm and its position in pixels is 655. Therefore, the new pixel/mm scale will be, 1pixel = 0.21mm.

This method is repeated three times for each image in order to have three points that describe the crack length. The first point is the origin of the crack (x_0, z_0) , the second point is that of the crack tip (x_f, z_f) , and the third point is located between the two points, (x_1, z_1) . Next, a second-order interpolation is carried out between the three points to consider the specimen curvature. Finally, the crack length, a , is calculated by integrating the obtained second-order fitting function, $f(x)$, between the origin and the end of the crack for each image:

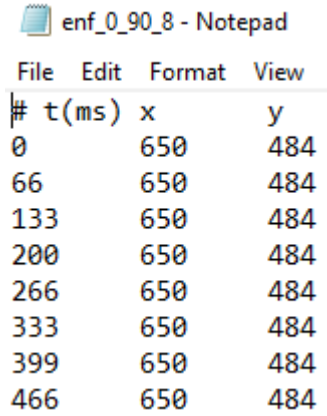
$$a = \int_{x_0}^{x_f} \sqrt{1 + f'(x)^2} dx \quad (3.1)$$

```

1  """
2  Code permettant de suivre le fond de fissure sur les videos AVI g n r es sur VIC
3  """
4
5  """ Remarques et am rliorations   faire dans le code
6  """
7  Am lioration   faire
8  """
9
10
11
12  """ Biblioth ques   importer
13  """
14  Import
15  """
16
17  #pip install moviepy
18  #pip install pygame ?
19  from moviepy.editor import VideoFileClip
20  from moviepy.video.tools.tracking import manual_tracking
21
22
23  #Chargement de la vid o - rentrer l'endroit ou se trouve les vid os + le nom de la video
24  Path_clip = 'C:/Users/Etel/Desktop/4ENF tests Python analysis/Analyses_specifiques/Fissure_tracking/'
25  Nom_essai = '0_90_15_dagApril19'
26
27  clip_video = VideoFileClip(Path_clip+Nom_essai+'.avi')
28  framerate=clip_video.fps
29
30  #Tracking manuel
31  trajectoires=manual_tracking(clip_video,t1=0, t2=clip_video.duration/framerate, nobjects=1, savefile=Nom_essai+'.txt')
32
33  # check 0-90-6

```

Figure 3-31: Python code used for crack monitoring.



#	t(ms)	x	y
0		650	484
66		650	484
133		650	484
200		650	484
266		650	484
333		650	484
399		650	484
466		650	484

Figure 3-32: Text file generated by the python script giving the crack length in pixels

Therefore, the provided python script for the analytical calculation of R-curve (critical strain energy releasing rate), can access each information of crack length propagation from the saved txt file which was determined through crack tip tracking and the scale on the conversion between pixels and millimeter is already included in the script and the crack length in the calculation is in millimeters.

3.4.4 Calculation of the strain energy releasing rate

The rate of critical strain energy releasing rate in mode-II can be calculated as different relevant variables have been determined. Therefore, we can apply the various approaches described in the bibliographic study, such as Compliance Calibration and Compliance Based Beam Methods, and then comparing the results found through applying different methods. results.

For the two methods, the compliance of the 4-ENF specimen must be first determined. The extracted displacement from VIC-3D software and the registered force from the load cell of the machine are used to find the compliance. Then, the two methods are applied to obtain the critical strain energy release rate and the final R-curves.

3.4.4.1 CCM: Compliance Calibration Method

First, the specimen compliance at each crack propagation is calculated:

$$C = \frac{\delta}{P} \quad (3.2)$$

The CCM method is based on the definition of a relationship between the specimen compliance and the crack length. In the case of 4ENF test, $C=f(a)$ is a linear function [14]. To find this function, the evolution of the compliance with the crack length (Figure 3.33) is fitted with a first order equation as follows:

$$C(a) = C_0 + C_1 a \quad (3.3)$$

The critical strain energy release rate can be calculated from the Irwin-Kies equation:

$$G_{IIc} = \frac{P^2}{2b} \frac{dC}{da} \quad (3.4)$$

Considering the linear distribution of the Compliance/crack length function of Equation 3.3, G_{IIc} can be calculated as follows:

$$G_{IIc} = \frac{C_1 P^2}{2b} \quad (3.5)$$

Where C_1 corresponds to the slope of the curve $C=f(a)$, found from the fitting equation. P is the applied load, provided by the test machine, and b , correspond to the specimen width, measured for each specimen.

Finally, the R-curve, which describes the evolution of the calculated critical strain energy at each crack propagation as a function of the corresponding crack length, can be plotted for each specimen, as depicted in Figure 3.34.

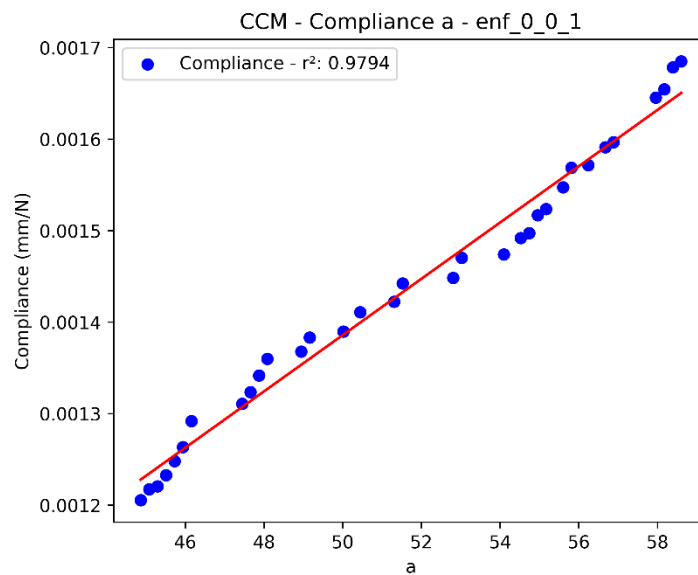


Figure 3-33: Example of the evolution of the specimen compliance as a function of the crack length.

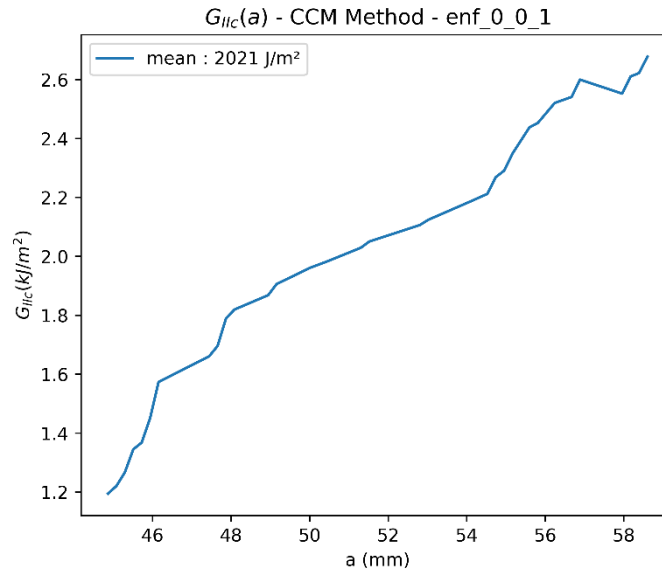


Figure 3-34: Example of the R-curve obtained with the Compliance Calibration Method.

3.4.4.2 CBBM: Compliance Based Beam Calibration Method

As its name indicates, the Compliance Based Beam Method uses beam theory to calculate the compliance for each crack length. To this end, the displacement equation at the two loading points determined by Martin and Davidson [14] is modified according to the dimensions of the 4ENF test setup and the size of the tested specimens. The displacement expression is then used to find the following Compliance expression:

$$C_{theo} = \left(\frac{23L^3}{1944.EI} + \frac{25L^2}{1944.EI} \right) + \frac{L^2}{12.EI} \cdot a \quad (3.6)$$

By combining Equation 3.4 and Equation 3.6, the critical strain energy release rate can be thereafter calculated as:

$$G_{IIc} = \frac{P^2 L^2}{24bEI} \quad (3.7)$$

The Young's modulus in Eqn. (3.7) is a parameter that can have significant variability from one specimen to another for a natural material such as wood. For this reason, it is more accurate to know the specific Young's modulus of each specimen tested. Within this context, De Moura et al. [15] suggested using the initial compliance corresponding to the initial crack, a_0 , to find Young's modulus for each specimen. This approach is adopted in this study, and the effective Young's modulus of each specimen is calculated from the following equation:

$$C_0 = \left(\frac{23L^3}{1944.EI} + \frac{25L^2}{1944.EI} \right) + \frac{L^2}{12.EI} \cdot a_0 \quad (3.8)$$

3.4.5 *Infrared thermography*

In order to see the energy releases caused by the development of the fracture, an infrared thermography apparatus was put up. The energy level captured were presumably low to make use of it under the analysis. Hence, if no useable data are produced from the rest of the techniques, the IR thermography will serve as a back up to conduct the analysis and better understand the way the specimen behave under certain loading conditions.

3.5 Conclusion

This chapter summarizes all the manufacturing process of the studied poplar plywood specimens. Moreover, a description of the 4ENF test was done. Thereafter, the two methods, CCM and CBBM used to compute the results of the fracture toughness behaviour are detailed. The results from the python script that permits the calculation of the fracture toughness by those two methods will be presented under the results section.

4. RESULTS AND DISCUSSION

4.1 Introduction

The data reduction technique was bearable to this work as there were more than 30 specimens in total for the 0/0 and 0/90 orientation. It starts from registering every necessary data of specimens so as to impute them in the analysis, a great care and focus must be given here as a single mistake could lead to a significant delusion of results which cannot represent the material. The validation of results done by comparing the experimental results with that of the analytical results. The following section elaborates steps that has been followed to find the Resistance-curve of the specimens.

4.2 Load-displacement responses

Figure 4.1 shows all the force-displacement curves for the seven 0°/0° and the ten 0°/90° specimens that are selected. In both cases, the curves show three different regions. First, the curve starts with a linear behaviour of force versus displacement up to an imposed displacement of 1.6 mm for 0°/0° and 1.4 mm for 0°/90° on average. In this linear part, the slope is constant, and no delamination is observed. Second, a non-linear behaviour begins when the force reaches a critical value, corresponding to the beginning of delamination. This is reflected by a change in the force-displacement curve's slope which consequently corresponds to a crack propagation. In fact, the decreasing slopes of the force-displacement curve corresponds to different compliances and corresponding crack propagation. During this propagation, the force is slightly increased in the 0°/0° case and is practically constant for 0°/90°, which is expected with a 4ENF test that promises stable crack propagation [14]. Finally, the curve shows a drastic drop in the force's value, corresponding to a total specimen failure.

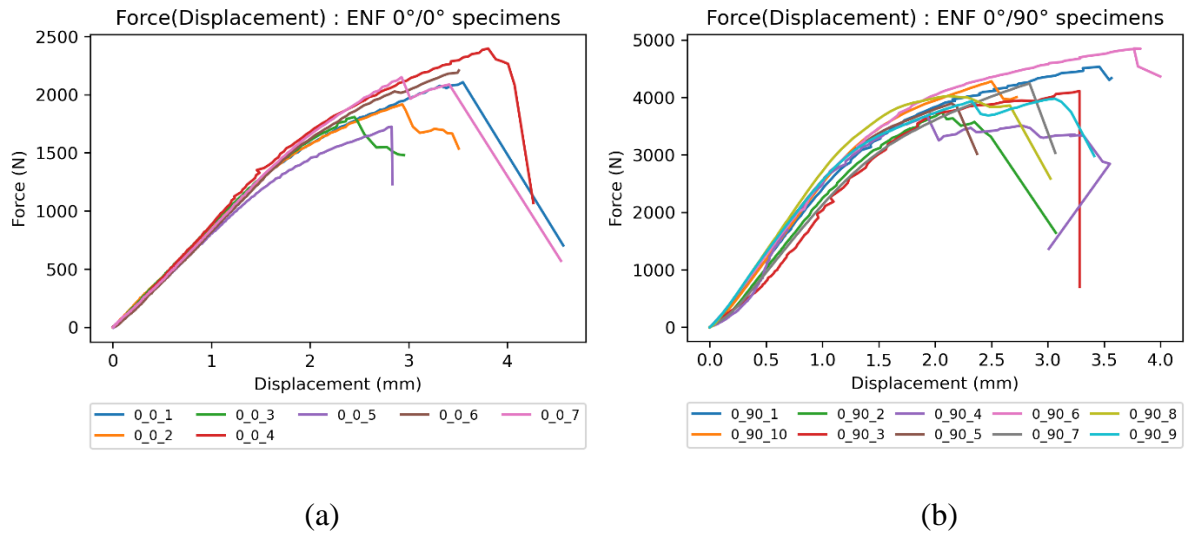


Figure 4-1: Evolution of the force with the displacement for (a) 0°/0° and (b) 0°/90° specimens.

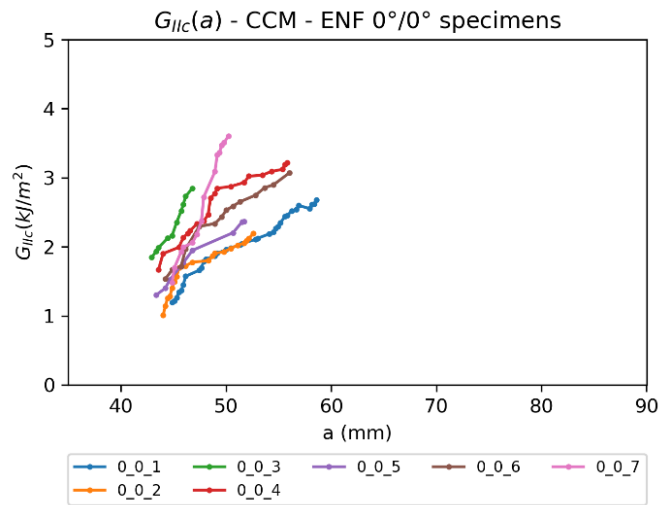
4.3 Resistance-curves

From the force-displacement curves, the compliance can be calculated according to the above equation. Then, Compliance Calibration Method, described in the second chapter, is adopted to calculate the critical energy releasing rate for each crack propagation, and to finally obtain the R-curves, depicted in Figure 4.2.

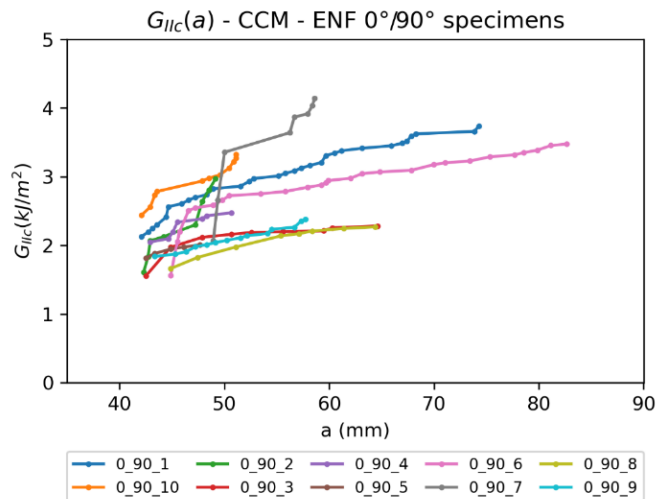
For the 0°/0° interface, the critical strain energy releasing rate increases with the crack propagation. The crack begins to propagate from the initial crack. Gradually, the crack continues to propagate in a smooth and stable manner until the final crack. During this propagation, G_{IIC} increases on average from 1.47 to 2.77 KJ/m² (an increase of about 88%) for approximately 13 mm of stable crack propagation. From all the tested 0°/0° specimens, an average G_{IIC} value of 2.21 KJ/m² is obtained. It should be noted that this value is calculated from the average G_{IIC} values of all the tested 0°/0° specimens, summarized in the below table 4.1. Each G_{IIC} value of a specimen in the table is calculated by averaging G_{IIC} over all the crack propagation. It can be concluded that the test has good repeatability. In fact, the coefficient of variation between G_{IIC} values is about 16.19%, which can be considered as acceptable for such a green material.

For the 0°/90° interface, the R-curves show the same behaviour as the 0°/0° specimens, i.e., G_{IIC} increases as the crack propagates, with an average value of 2.50 KJ/m² (Table 4.2). However, the trend of increasing in G_{IIC} from the initial to the final crack length is less remarkable than for the 0°/0° interface. Indeed, during the propagation, G_{IIC} increases from 1.92 to 2.98 KJ/m² in 28 mm of stable crack propagation. This represents an increase in G_{IIC} of

55%, i.e., lower increment than the $0^\circ/0^\circ$ interface. This less remarkable increment reflects greater and smoother propagation for the $0^\circ/90^\circ$ interface. Theoretically, the critical strain energy releasing rate does not depend on crack length and remains constant throughout propagation. One of the effects that can influence the evolution of G_{IIc} is the friction between the two interface surfaces [31], [32]. Indeed, as the crack propagates, the contact surface at the interface increases, so friction becomes more important, which may require more energy to continue propagating the crack.



(a)



(b)

Figure 4-2: R-curves for (a) $0^\circ/0^\circ$ and (b) $0^\circ/90^\circ$ specimens obtained with Compliance Calibration Method.

Table 4-1: Mean critical strain energy release rates of 0°/0° specimens.

Specimens	G_{IIc} (CCM)	G_{IIc} (CBBM)	Relative error (%)
0-0-1	2021	1512	25.18
0-0-2	1715	1289	24.83
0-0-3	2312	1339	42.08
0-0-4	2605	2094	19.61
0-0-5	1859	1140	38.67
0-0-6	2378	1685	29.14
0-0-7	2628	1803	31.39
Average (J/m ²)	2216.85	1551.71	30.13
CoV. (%)	16.19	21.37	

Table 4-2: Mean critical strain energy release rates of 0°/90° specimens.

Specimens	G_{IIc} (CCM)	G_{IIc} (CBBM)	Absolute Relative error (%)
0-90-1	3008	2794	7.11
0-90-2	2293	1923	16.13
0-90-3	2104	2619	24.47
0-90-4	2280	2091	8.28
0-90-5	1925	2679	39.16
0-90-6	2889	3379	16.96
0-90-7	3459	2708	21.71
0-90-8	2061	2098	1.79
0-90-9	2098	2388	13.82
0-90-10	2944	2662	9.57
Average (J/m ²)	2506.10	2534.10	15
CoV. (%)	20.85	16.83	

4.4 Discussion

In this section, we first compare the experimental values from the CCM method to the analytical method (CBBM), to validate the obtained results. Next, an attempt is made to analyse the causes behind the differences in the fracture toughness found between 0°/0° and 0°/90° interfaces, based on images of the fracture interfaces surfaces. Finally, attention is given to the comparison of the mode II with the mode I fracture toughness results, to understand the behaviour of poplar plywood under the most possible fracture conditions.

4.4.1 Comparison of the fracture toughness calculated with CCM and CBBM

Figure 4.3 depicts the results of the main critical energy releasing rate calculated by means of the two methods (detailed values are summarized in Table 4.1 and 4.2). As it can be seen in the Figure, a good agreement is found between Compliance Calibration and Compliance Based Beam Methods. Also, the relative error between CCM and CBBM is more significant for the $0^\circ/0^\circ$ interface and it is about 30% on average, compared to approximately 15% averaged over all the $0^\circ/90^\circ$ specimens' relative errors. This can be explained by the fact that the $0^\circ/90^\circ$ specimens has longer crack propagation length and smoother crack propagation than the specimens with $0^\circ/0^\circ$ specimens. Hence, G_{IIC} values are closer to the analytical method for $0^\circ/90^\circ$ specimens.

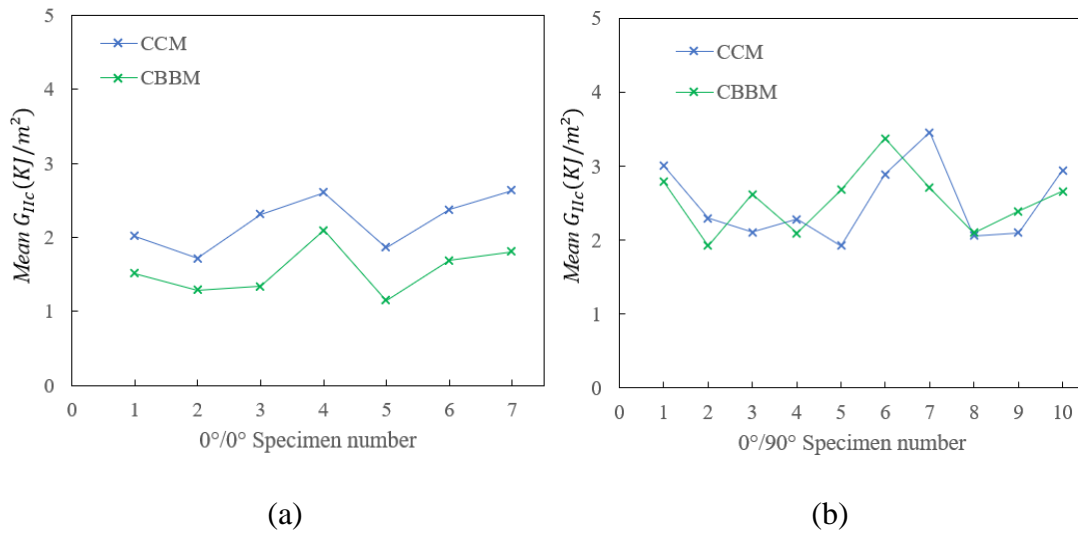


Figure 4-3: Mean values of G_{IIC} obtained with CCM and CBBM for (a) $0^\circ/0^\circ$ and (b) $0^\circ/90^\circ$ specimens.

4.4.2 Comparison of mode II delamination between $0^\circ/0^\circ$ and $0^\circ/90^\circ$ interfaces

A comparison of the R-curves (depicted in Figure 4.2) between the two studied interfaces, reveals two major differences. First, propagation is greater for specimens with a $0^\circ/90^\circ$ interface. Indeed, the crack propagation length in this case is averagely about 28 mm, which is more than the double of specimens with the $0^\circ/0^\circ$ interface (about 13 mm on average). Second, the mean G_{IIC} value is slightly higher for specimens with $0^\circ/90^\circ$ interface than those with $0^\circ/0^\circ$ interface. In fact, the mean of G_{IIC} for $0^\circ/90^\circ$ interface is about 2.5 KJ/m², which is ~13% higher than G_{IIC} for $0^\circ/0^\circ$ interface.

This increase in G_{IIC} value while increasing the interface angle of ply orientation has also been observed for composite materials. For example, Perreira et al. [33] have studied mode II delamination of carbon/epoxy composites with $0/\theta$ interfaces and have found that the fracture toughness increased with increasing the θ value. They found a G_{IIC} equal to 1.6 and 1.1 for $0^\circ/90^\circ$ and $0^\circ/0^\circ$ interfaces, respectively. Hiley et al. [34] and Gong et al. [35] have also found the same trend for carbon-epoxy composites with $0^\circ/0^\circ$, $0^\circ/45^\circ$ and $0^\circ/90^\circ$ interfaces.

To better explain this difference, an analysis of the delamination growth path and the fracture surfaces of the $0^\circ/0^\circ$ and $0^\circ/90^\circ$ interfaces is carried out. The figure 4.4 and 4.5 show the delamination growth path in $0^\circ/0^\circ$ and $0^\circ/90^\circ$ interfaces, respectively. In the case of $0^\circ/0^\circ$ interface, the crack propagates along the interface between the two 0° plies without jumping in other plies. However, for the $0^\circ/90^\circ$ interface, the crack propagates strictly within the 90° ply and the delamination path is quite complex. In fact, the crack propagates in a tortuous manner between the 90° oriented fibres of the 90° ply (Figure 4.6). This complex delamination path absorbs more energy to allow further crack propagation. Moreover, the fibres of the 90° ply create toughening effects as they are perpendicular to the delamination path., which can be an additional source of energy absorption. The figures 4.7 and 4.8 show the fracture surfaces for $0^\circ/0^\circ$ and $0^\circ/90^\circ$ interfaces, respectively. To get a better view of the fracture surfaces, the specimens were opened by hand. In the case of $0^\circ/0^\circ$ interface, the fracture surfaces are very smooth. Indeed, the crack propagates in the direction of the fibres, which may facilitate its growth. For the $0^\circ/90^\circ$ interface, the fracture interface is more complicated. The fracture propagates in the 90° ply, i.e., in a direction perpendicular to the fibres. The fracture surface is larger than the $0^\circ/0^\circ$ one with localised fibre breakage. This fibre breakage behaviour was not encountered in the $0^\circ/0^\circ$ case and it can be a major energy release source during the fracture process.

All these phenomena observed for $0^\circ/90^\circ$ fracture interface can be a significant sources of energy release. So, $0^\circ/90^\circ$ specimens require greater energy to continue delaminating perpendicular to the fibres, compared to $0^\circ/0^\circ$ specimens. Consequently, G_{IIC} is higher for $0^\circ/90^\circ$ than for $0^\circ/0^\circ$ interface.

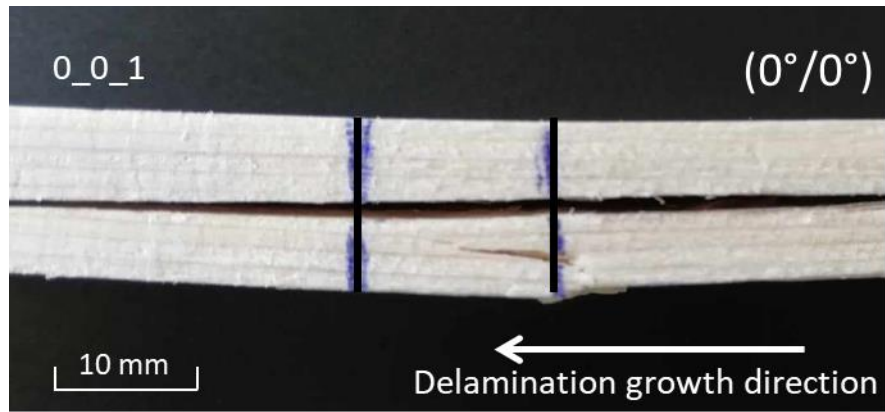


Figure 4-4: Side view of the delamination growth in $0^\circ/0^\circ$ interface.



Figure 4-5: Side view of the delamination growth in $0^\circ/0^\circ$ and in (b) $0^\circ/90^\circ$ interface.

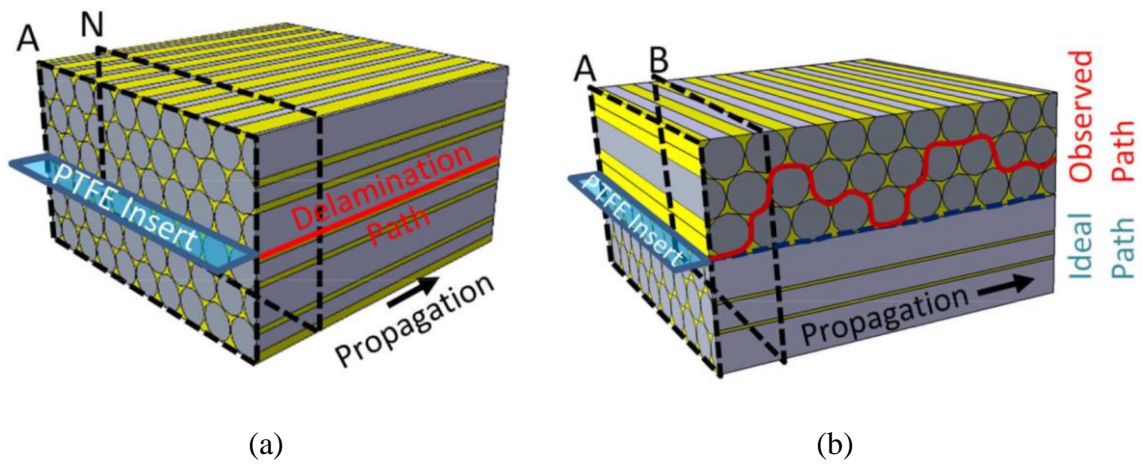


Figure 4-6: Delamination path for (a) $0^\circ/0^\circ$ and (b) $0^\circ/90^\circ$ specimens [36], [37].

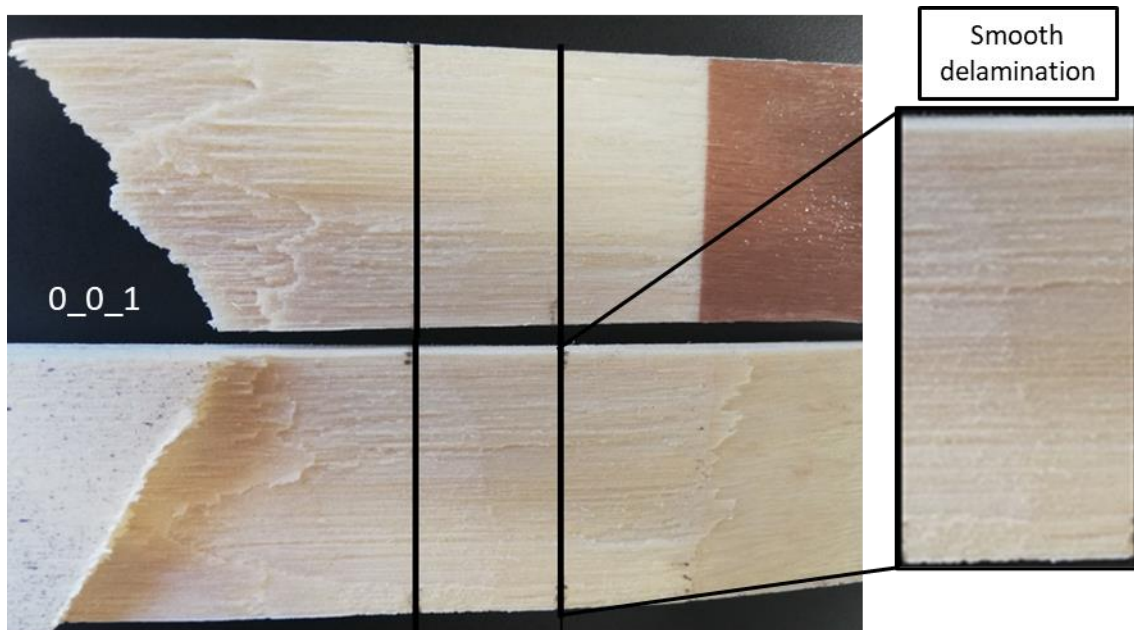


Figure 4-7: Fracture surfaces of a specimen with a $0^\circ/0^\circ$ interface.

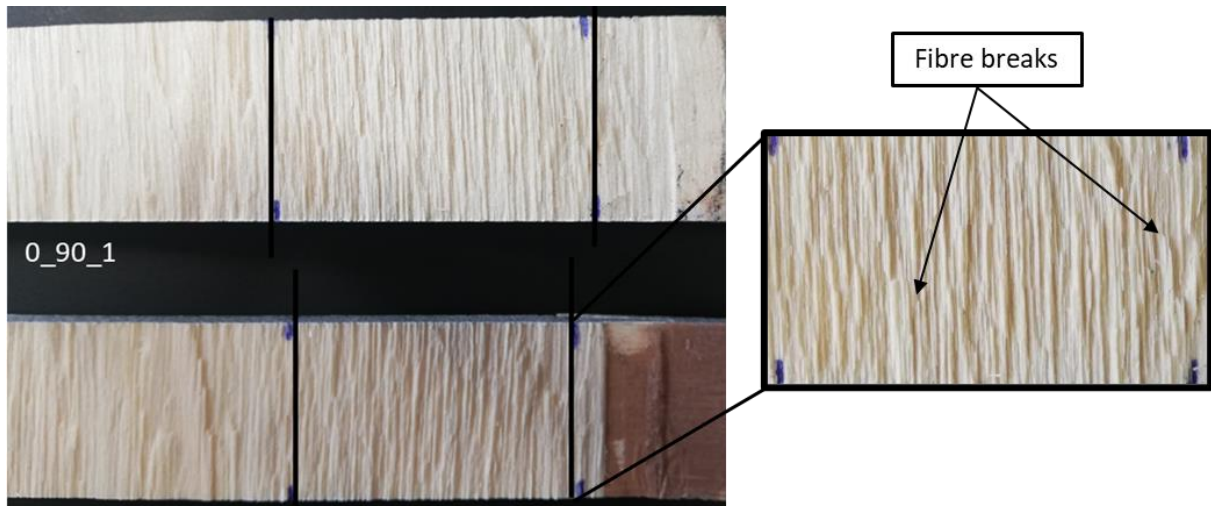


Figure 4-8: Fracture surfaces of a specimen with a $0^\circ/90^\circ$ interface.

4.4.3 Mode II and mode I fracture toughness

As mentioned in the second chapter, the Mode I of poplar plywood was also studied as part of the same project. The results showed that the G_{Ic} value is about 0.4 and 0.2 KJ/m^2 for $0^\circ/0^\circ$ and $0^\circ/90^\circ$ interfaces, respectively [38]. The G_{IIc} in mode II is therefore 5 times to 12 times greater than that of in mode I. This can be explained by the phenomenon of planar delamination in mode II, which is different from the opening phenomenon in mode I and may require more energy to propagate a crack. In fact, the tensile stress perpendicular to the fibres is lower in the mode I, compared to the mode II loading. So, the force required to open the specimen is lower. Less energy is therefore required to propagate the crack for the mode I loaded specimens. This

result agrees with literature results for solid wood, LVL or composite materials (Table 4.3). However, no clear trend can be drawn from the ratio between mode II and mode I fracture toughness. Indeed, this ratio is very dependent on the nature of the material and the characteristics of reinforcement fibres (wood or synthetic fibres).

Table 4-3: Mode I and mode II fracture toughness of poplar plywood compared to wood and composite materials from the literature.

Material	$G_{Ic}(KJ/m^2)$	$G_{IIc}(KJ/m^2)$	G_{IIc}/G_{Ic}
Current study (0°/0°)	0.4	2.1	5.25
Current study (0°/90°)	0.2	2.5	12.50
Radiata pine LVL [24]	0.67	4.01	5.96
Radiata pine timber [24]	0.49	6.96	14.20
Pinus Pinaster [39]	0.34	2.51	7.38
Spruce massive wood [40]	0.18	0.74	4.11
Carbon/epoxy [41]	0.5	1.6	3.2
UD glass-E/polyester [42]	0.40	0.74	1.85

4.5 Conclusion

With the lack of literature works on the interfacial fibre direction influence on mode II fracture toughness of wood and wood composites, the current work presents for the first time a detailed quantification of G_{IIc} considering two different interfaces: 0°/0° and 0°/90° of poplar plywood, tested under mode II loading by means of Four-point End Notched Flexure tests. The results reveal an increase in G_{IIc} for 0°/90° compared to 0°/0° interface. Analysis of the fracture interface show different delamination paths in the two cases: a propagation of the crack at the interface between the two 0° plies (for 0°/0° interface specimens) or within the 90° ply (for 0°/90° interface specimens). Moreover, the aspect of the fracture surfaces is another important factor affecting delamination resistance. The complex crack propagation between the 90° fibres and their breakage in the 0°/90° interface, as well as the high resistance of the 90° fibres, perpendicular to the delamination path, were found to be a very important energy dissipation mechanisms that explain the highest G_{IIc} for 0°/90° compared to 0°/0° interface. An analytical method (Compliance Based Beam Method) was also deployed to calculate the fracture toughness in both cases: 0°/0° and 0°/90° interfaces, and a good agreement was found with the experimental results.

This study gave a quantification of the Mode II fracture toughness of poplar plywood, while investigating the effect of the increment in angle of orientation of fibres at the interface, which creates energy absorption mechanisms that result in higher toughness. The values obtained in this study and in the previous Mode I study provide the fracture toughness values needed to be implemented in a numerical model developed within the research team in the ICA (DPM: Discrete Ply Model [43]–[45]). This will enable the prediction of failure at the scale of structural components and open design opportunities for more damage-tolerant wood composites.

REFERENCES

- [1] B. Castanie, C. Bouvet, and M. Ginot, ‘Review of composite sandwich structure in aeronautic applications’, *Compos. Part C Open Access*, vol. 1, p. 100004, Aug. 2020.
- [2] J. Sutherland, ‘Revival of structural timber in Britain after 1945’, 2023.
- [3] A. Klemin, ‘Aviation Surveyed’, *Sci. Am.*, vol. 170, no. 5, pp. 214–216, May 1944.
- [4] J. Susainathan and F. Eyma, ‘Wood Based Composite Sandwich Structures’, 2018.
- [5] U. Müller *et al.*, ‘Crash simulation of wood and composite wood for future automotive engineering’, *Wood Mater. Sci. Eng.*, vol. 15, no. 5, pp. 312–324, Sep. 2020.
- [6] A. Elmendorf, ‘PLYWOOD AND ITS USES IN AUTOMOBILE CONSTRUCTION’, presented at the Pre-1964 SAE Technical Papers, Jan. 1920, p. 200037.
- [7] ‘[https://fr.wikipedia.org/wiki/%C3%89ole_\(avion\)](https://fr.wikipedia.org/wiki/%C3%89ole_(avion))’.
- [8] ‘<https://www.thomasnet.com/insights/a-brief-history-of-aircraft-materials/>’.
- [9] G. T. Tsoumis, ‘<https://www.britannica.com/science/wood-plant-tissue>’, Encyclopedia Britannica, Mar. 2023.
- [10] M. Turis and O. Ivánková, ‘Using finite element analysis to obtain plastic zones in the vicinity of the crack edges, under mixed mode loading conditions’, *MATEC Web Conf.*, vol. 310, p. 00028, 2020.
- [11] P. Davies, ‘Review of standard procedures for delamination resistance testing’, in *Delamination Behaviour of Composites*, Elsevier, 2008, pp. 65–86. doi: 10.1533/9781845694821.1.65.
- [12] X. Liu, T. Sun, Z. Wu, and H. He, ‘Mode II interlaminar fracture toughness of unidirectional fiber-reinforced polymer matrix composites with synthetic boehmite nanosheets at room temperature and low temperature’, *J. Compos. Mater.*, vol. 52, no. 7, pp. 945–952, Mar. 2018.
- [13] H. Wang and T. Vu-Khanh, ‘Use of end-loaded-split (ELS) test to study stable fracture behaviour of composites under mode II loading’, *Compos. Struct.*, vol. 36, no. 1–2, pp. 71–79, Sep. 1996.
- [14] R. H. Martin and B. D. Davidson, ‘Mode II fracture toughness evaluation using four point bend, end notched flexure test’, *Plast. Rubber Compos.*, vol. 28, no. 8, pp. 401–406, Aug. 1999.
- [15] K. Tanaka, T. Yuasa, and K. Katsura, ‘Continuous mode II interlaminar fracture toughness measurement by over notched flexure test.’, *4 Th Eur. Conf. Compos. Test. Stand.*, pp. 171–179, 1998.
- [16] W.-X. Wang, M. Nakata, Y. Takao, and T. Matsubara, ‘Experimental investigation on test methods for mode II interlaminar fracture testing of carbon fiber reinforced composites’, *Compos. Part Appl. Sci. Manuf.*, vol. 40, no. 9, pp. 1447–1455, Sep. 2009.
- [17] P. Davies *et al.*, ‘Comparison of test configurations for determination of mode II interlaminar fracture toughness results from international collaborative test programme’, *Plast. Rubber Compos.*, vol. 28, no. 9, pp. 432–437, Sep. 1999.
- [18] H. Yoshihara and M. Ohta, ‘Measurement of mode II fracture toughness of wood by the end-notched flexure test’, *J. Wood Sci.*, vol. 46, no. 4, pp. 273–278, Aug. 2000.
- [19] O. Laban and E. Mahdi, ‘Enhancing mode I inter-laminar fracture toughness of aluminum/fiberglass fiber-metal laminates by combining surface pre-treatments’, *Int. J. Adhes. Adhes.*, vol. 78, pp. 234–239, Oct. 2017.
- [20] M. F. S. F. de Moura, M. A. L. Silva, J. J. L. Morais, and N. Dourado, ‘Mode II fracture characterization of wood using the Four-Point End-Notched Flexure (4ENF) test’, *Theor. Appl. Fract. Mech.*, vol. 98, pp. 23–29, Dec. 2018.

-
- [21] H. Yoshihara, ‘Resistance curve for the mode II fracture toughness of wood obtained by the end-notched flexure test under the constant loading point displacement condition’, *J. Wood Sci.*, vol. 49, no. 3, pp. 210–215, Jun. 2003.
- [22] H. Yoshihara, ‘Mode II R-curve of wood measured by 4-ENF test’, *Eng. Fract. Mech.*, vol. 71, no. 13–14, pp. 2065–2077, Sep. 2004.
- [23] H. Yoshihara, ‘Theoretical analysis of 4-ENF tests for mode II fracturing in wood by finite element method’, *Eng. Fract. Mech.*, vol. 75, no. 2, pp. 290–296, Jan. 2008.
- [24] B. Franke and P. Quenneville, ‘Analysis of the fracture behavior of Radiata Pine timber and Laminated Veneer Lumber’, *Eng. Fract. Mech.*, vol. 116, pp. 1–12, Jan. 2014.
- [25] A. El Moustaphaoui, A. Chouaf, and K. Kimakh, ‘Experimental and numerical study of the delamination of Ceiba plywood under mode I, mode II and mixed-mode (I + II) loading using the DCB, ELS and MMF tests’, *Int. J. Fract.*, Jun. 2021.
- [26] A. EL Moustaphaoui, A. Chouaf, M. Chergui, and K. Kimakh, ‘Modeling of macroscopic delamination of plywood using design of experiments method’, *J. Indian Acad. Wood Sci.*, vol. 16, no. 2, pp. 144–154, Dec. 2019.
- [27] A. El Moustaphaoui, A. Chouaf, K. Kimakh, and M. Chergui, ‘Determination of the onset and propagation criteria of delamination of Ceiba plywood by an experimental and numerical analysis’, *Wood Mater. Sci. Eng.*, vol. 16, no. 5, pp. 325–335, Sep. 2021.
- [28] ‘<https://www.woodmagazine.com/wood-supplies/lumber/what-veneer-patterns-are-available-for-plywood>’.
- [29] P. Reu, ‘All about speckles: Speckle Size Measurement’, *Exp. Tech.*, vol. 38, no. 6, pp. 1–2, 2014.
- [30] T. Triantafillou, *Textile Fibre Composites in Civil Engineering*. Woodhead Publishing, 2016.
- [31] B. D. Davidson and X. Sun, ‘Effects of Friction, Geometry, and Fixture Compliance on the Perceived Toughness from Three-and Four-Point Bend End-Notched Flexure Tests’, *J. Reinf. Plast. Compos.*, vol. 24, no. 15, pp. 1611–1628, Oct. 2005.
- [32] B. D. Davidson, X. Sun, and A. J. Vinciguerra, ‘Influences of Friction, Geometric Nonlinearities, and Fixture Compliance on Experimentally Observed Toughnesses from Three and Four-point Bend End-notched Flexure Tests’, *J. Compos. Mater.*, vol. 41, no. 10, pp. 1177–1196, May 2007.
- [33] A. B. Pereira, A. B. de Moraes, A. T. Marques, and P. T. de Castro, ‘Mode II interlaminar fracture of carbon/epoxy multidirectional laminates’, *Compos. Sci. Technol.*, vol. 64, no. 10–11, pp. 1653–1659, Aug. 2004.
- [34] M. J. Hiley, ‘Delamination between multi-directional ply interfaces in carbon-epoxy composites under static and fatigue loading’, in *European Structural Integrity Society*, Elsevier, 2000, pp. 61–72. doi: 10.1016/S1566-1369(00)80008-4.
- [35] Y. Gong, K. Xia, Y. Wang, L. Zhao, J. Zhang, and N. Hu, ‘A semi-analytical model for the mode II fracture toughness of multidirectional composite laminates’, *Thin-Walled Struct.*, vol. 182, p. 110235, Jan. 2023.
- [36] A. Ramji, Y. Xu, M. Yasaei, M. Grasso, and P. Webb, ‘Delamination migration in CFRP laminates under mode I loading’, *Compos. Sci. Technol.*, vol. 190, p. 108067, Apr. 2020.
- [37] A. Ramji, Y. Xu, M. Grasso, M. Yasaei, and P. Webb, ‘Effect of interfacial fibre orientation and PPS veil density on delamination resistance of 5HS woven CFRP laminates under mode II loading’, *Compos. Sci. Technol.*, vol. 207, p. 108735, May 2021.
- [38] A. Peignon, J. Serra, L. Gélard, A. Cantarel, F. Eyma, and B. Castanié, ‘Mode I delamination R-curve in poplar laminated veneer lumber’, *Theoretical and Applied Fracture Mechanics*, p. 103982, Aug. 2023.

-
- [39] J. Xavier, J. Morais, N. Dourado, and de M. F. S. F. Moura, 'Measurement of Mode I and Mode II Fracture Properties of Wood-Bonded Joints', *J. Adhes. Sci. Technol.*, vol. 25, no. 20, pp. 2881–2895, Jan. 2011.
- [40] R. Putzger and P. Haller, 'Fracture Energy in Mode I and Mode II of Textile Reinforced Wood', in *Fracture of Nano and Engineering Materials and Structures*, E. E. Gdoutos, Ed., Dordrecht: Springer Netherlands, 2006, pp. 453–454.
- [41] S. Rivallant, C. Bouvet, and N. Hongkarnjanakul, 'Failure analysis of CFRP laminates subjected to compression after impact: FE simulation using discrete interface elements', *Compos. Part Appl. Sci. Manuf.*, vol. 55, pp. 83–93, Dec. 2013.
- [42] A. Szekrényes, 'Prestressed fracture specimen for delamination testing of composites', *Int. J. Fract.*, vol. 139, no. 2, pp. 213–237, May 2006.
- [43] C. Bouvet, J. Serra, and P. G. Perez, 'Strain rate effect of mode II interlaminar fracture toughness on the impact response of a thermoplastic PEEK composite', *Composites Part C: Open Access*, p. 100031, Oct. 2020.
- [44] J. Serra, A. Trelu, C. Bouvet, S. Rivallant, B. Castanié, and L. Ratsifandrihana, 'Combined loadings after medium velocity impact on large CFRP laminated plates: Discrete ply model simulations', *Compos. Part C Open Access*, vol. 6, p. 100203, Oct. 2021.
- [45] P. Journoud, C. Bouvet, B. Castanié, and L. Ratsifandrihana, 'Numerical analysis of the effects of wrinkles in the radius of curvature of L-shaped CFRP specimens on unfolding failure', *Compos. Struct.*, p. 116107, Nov. 2022.